Synthesis, characterization, anti-tuberculosis activity and molecular modeling studies of thiourea derivatives bearing aminoguanidine moiety

Michael Tapera, Hüseyin Kekeçmuhammed, Kader Sahin, Vagolu Siva Krishna, Christian Lherbet, Håvard Homberset, Mélina Chebaiki, Tone Tønjum, Lionel Mourey, Yunus Zorlu, et al.

Synthesis, characterization, anti-tuberculosis activity and molecular modeling studies of thiourea derivatives bearing aminoguanidine moiety

Michael Tapera [a], Hüseyin Kekeçmuhammed [a], Kader Sahin [b], Vagolu Siva Krishna [c], Christian Lherbet [e], Håvard Homberset [c], Mélina Chebaiki [e,f], Tone Tønjum [c,d], Lionel Mourey [f], Yunus Zorlu [g], Serdar Durdagi [b], Emin Sarıpınar [a,*]

[a]*Department of Chemistry, Faculty of Science, Erciyes University, Melikgazi, 38039, Kayseri, Turkey*

[b]*Computational Biology and Molecular Simulations Laboratory, Department of Biophysics, School of Medicine, Bahcesehir University, Istanbul, Turkey*

[c]*Unit for Genome Dynamics, Department of Microbiology, University of Oslo, Oslo, Norway*

[d]*Division of Laboratory Medicine, Department of Microbiology, Oslo University Hospital, Oslo, Norway.*

[e]*LSPCMIB, UMR-CNRS 5068, université Paul Sabatier-Toulouse III, 118, route de Narbonne, 236 Cours Eugené Cosserat, 31062, Toulouse Cedex, France*

[f]*Institut de Pharmacologie et de Biologie Structurale, IPBS, Université de Toulouse, CNRS, UPS, Toulouse, France.*

[g]*Department of Chemistry, Gebze Technical University, Kocaeli 41400, Turkey*

**Corresponding author*

Prof. Dr Emin SARIPINAR

Address: Erciyes University

Department of Chemistry

Faculty of Science

38039

Kayseri, TURKEY

E-mail address: emin@erciyes.edu.tr

Phone number: +90 352 207 6666

Abstract

The emergence of drug-resistant *Mycobacterium tuberculosis* strains has posed a driving demand in the search for more effective treatment regimens for tuberculosis. In the present study, a series of novel thiourea derivatives containing aminoguanidine were synthesized by the condensation reaction of aminoguanidine and various isothiocyanates in an attempt to discern new potent active agents against tuberculosis. The structure of synthesized compounds was characterized by FTIR, ^{1}H-NMR, ^{13}C-NMR and HRMS. The proposed structure of compound **BI19** was resolved using single X-ray crystallography. The compounds were tested *in vitro* against MTB H37Rv for antitubercular activity. Some of them have high antimycobacterial action, for instance, **BI-17** with a MIC value of 1.3 μM and low cytotoxicity. Furthermore, computational studies and enzyme inhibition experiments were performed to identify the target for the observed antitubercular effects.

Keywords

Synthesis, thiourea, tuberculosis, computational investigations, InhA

1. Introduction

Tuberculosis (TB) is one of the most prevalent and deadly infectious diseases. TB is caused by a family of mycobacteriaceae pathogenic bacteria [1,2]. According to World Health Organization (WHO) report, a large number of deaths throughout the world are a result of the spread of TB disease caused by a single infectious bacterium [3]. In spite of the availability of various commercial anti-TB drugs, the disease continues to kill a large number of people around the world. The traditional medications' low efficacy against severely drug-resistant and multidrug-resistant TB exacerbates the treatment of TB [4]. Hence, new treatment medicines with lower toxicity profiles are urgently needed to combat the spread of tuberculosis.

Compounds with guanidine functionalities are present in a wide range of biologically relevant compounds, and they have lately been recognized as favored functional groups in the design and development of antibacterial drugs [5]. The great interest in this moiety stems mostly from their ability to be protonated at physiological pH leading to positively charged drugs which favors the binding to bacterial targets causing disruption of cell membranes and cell walls [6,7]. Many commercially available drugs in Figure 1, such as streptomycin and trimethoprim as antibiotics and progunil as an antimalarial, have a guanidine scaffold that is typically critical to their biological activity [8]. Furthermore, compounds with guanidine derivatives such as aminoguanidine have been reported as active compounds against numerous diseases. For example, robenidine (compound **1** in Figure 1), formerly called robenzidine, has been reported to display significant activity as gram-positive and gram-negative antibacterial agent [9,10]. In 2021, Krollenbrock *et al.* reported excellent activity of aminoguanidines (robenidine) against drug-resistant malaria *in vitro* and impressive *in vivo* efficacy with an ED_{50} (median effective dose) value of 0.25 mg/kg/day in a standard 4-day test [11]. In addition, aminoguanidine carrying compound **2** in Figure 1, was reported to have potent anti-TB with a substantial MIC (Minimal Inhibitory Concentration) value of 6.42 μM [12].

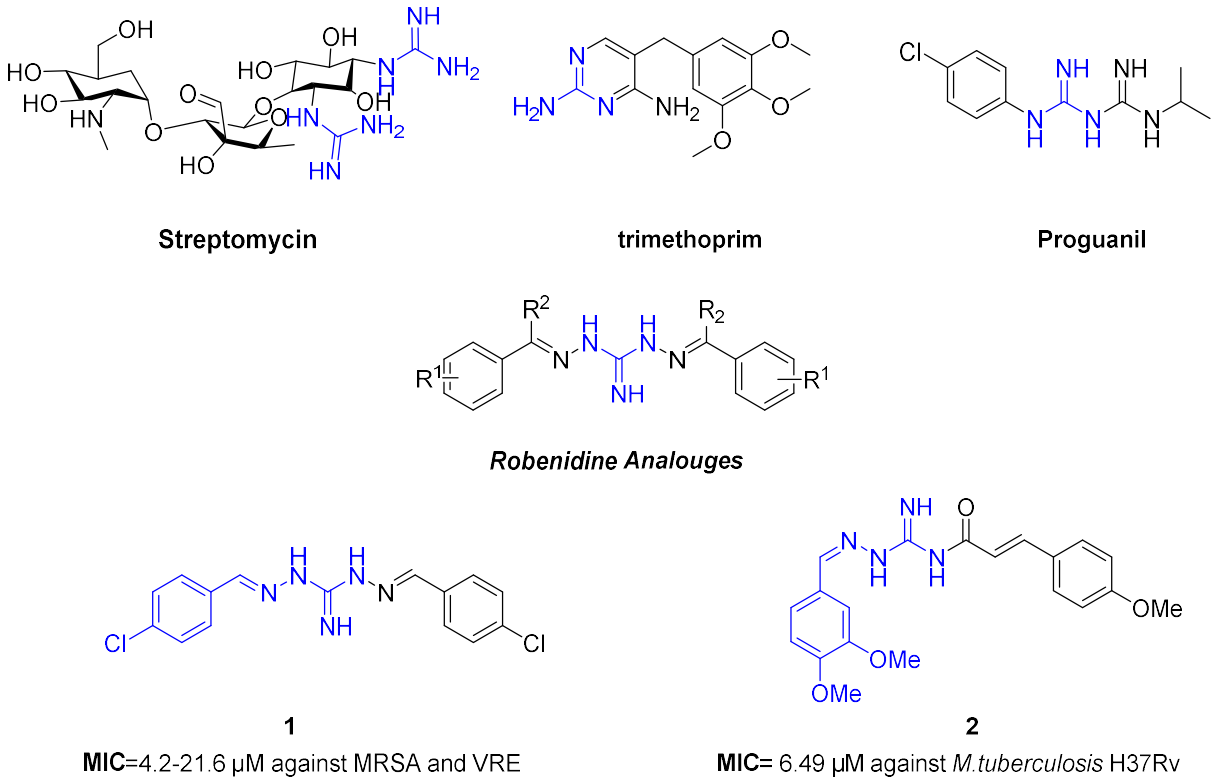

Fig. 1. Commercial antibacterial drugs and biologically active compounds containing guanidine moiety. In Fig. 1, Analogues and analouges and "trimethoprim" with an uppercase T: Trimethoprim

Similarly, compounds with hydrazide-hydrazone structural motifs have been reported to exhibit notable anti-TB activity [13,14], as well as activities against other infectious diseases like cholera and malaria [15,16]. Incorporating the hydrazone moiety into the structure of new therapeutic candidates as well as existing antimycobacterial drugs such as isoniazid and pyrazinamide is a feasible and widely used strategy for developing novel antitubercular compounds with lower toxicity (Figure 2) [17,18].

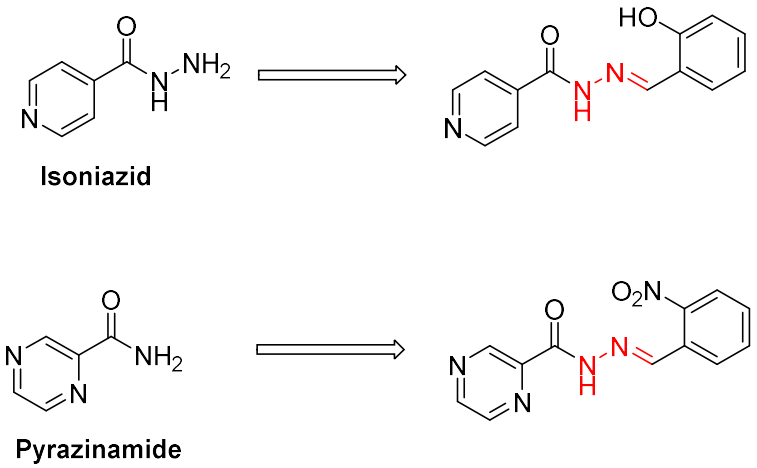

Fig. 2. Hydrazone derivatives of well-known antitubercular drugs that are antimycobacterial.

We have previously exploited hydrazone containing thiadiazoles derivatives, as *Mycobacterium tuberculosis* (MTB) growth and enoyl acyl carrier protein reductase (InhA) inhibitors. Molecules in this study displayed remarkable antimycobacterial activity, MIC=0.78-6.25 mg/mL, with low cytotoxicity [19].

Thiourea is a bioisostere of urea functionality in which the oxygen atom is substituted by a sulfur atom. It is one of the most important core structures in pharmaceutical chemistry [20]. This scaffold is a critical component in the development of novel drug candidates with a wide range of therapeutic applications. Many commercial examples include thioacetazone, thiocarlide (isoxyl) and noxytiolin all of which have the thiourea group incorporated into their structures (Figure 3), [21].

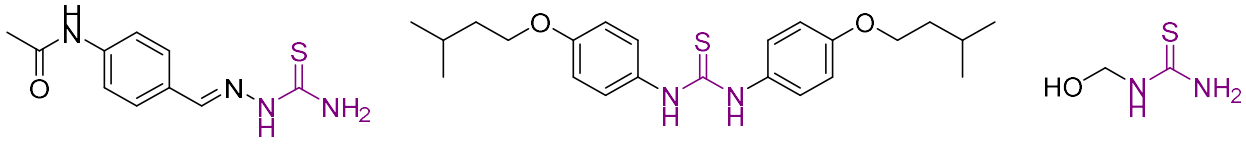

Fig. 3. Commercially available antibacterial drugs with thiourea moiety. Thiocarlide

Thioacetazone and thiocarlide (isoxyl) are thiourea-containing drugs that have been shown to be effective antitubercular drugs against MTB strains that are multidrug-resistant. They affect the synthesis of mycolic acid by interfering with the synthesis of oleic acid [22]. Their mode of action for limiting oleic acid synthesis has just been identified, and it involves covalently inhibiting the HadA component of MTB fatty acid synthase type II (FAS-II) dehydratase via the sulfur atom of thioketone functionality [23]

The mycobacterial cell envelope consists of long-chain fatty acids which are alpha branched and beta hydroxylated as part of their major component. These long-chain fatty acids are called mycolic acids and are responsible to make the bacteria less susceptible to antibiotics by making the cell envelope very complex and poorly permeable. Biosynthesis of mycolic acids is regulated by two elongation systems: fatty acid synthase type I (FAS-I) and type II (FAS-II). The FAS-II enzymes are viable targets for drug development because eukaryotic cells only use a FAS-I enzyme to synthesize fatty acids. The enoyl-acyl carrier protein (ACP) reductase, InhA, is a key enzyme in the mycolic acid biosynthesis pathway (FAS-II) of MTB. InhA is essential for the growth of MTB making it a promising target for the development of new antitubercular agents [24].

Antitubercular drug, isoniazid (INH), is a prodrug that has to be activated by the catalase-peroxidase enzyme KatG. INH, after activation, forms an INH-NAD adduct which inhibits InhA. Clinical resistances to INH are predominantly due to mutations within KatG. Then, different classes of direct inhibitors of InhA, which do not require pre-activation by KatG, were discovered [25]. The active site of InhA, buried in a large cavity, could accommodate various inhibitors such as aryl amide, thiazole urea, macrocyclic biaryl ether or pyridomycin lately [26–29].

In view of these considerations, we synthesized thiourea derivatives bearing aminoguanidine moiety to inhibit MTB growth and InhA inhibitors. To evaluate these compounds, we performed MTB assays, molecular modeling studies to evaluate the possible binding mode of our inhibitors and finally measurements of InhA enzyme inhibition.

2. Results and discussion

2.1. Chemistry

The target compounds were synthesized according to the procedures shown in Scheme 1. The condensation reaction of commercially available substituted benzaldehydes or acetophenones (**1**)

with 1,3-diaminoguanidine hydrogen chloride to afford robenidine analogues **3**. Robenidine analogues **3** were obtained in salt form with hydrogen chloride, there were neutralized by utilizing an inorganic base potassium hydroxide using mole equivalent of 1,3-diaminoguanidine **2**. Targeted compounds **BI** (**1-25**) were synthesized according to the modified literature procedure [30] by reacting robenidine analogues **3** in presence of substituted phenyl isothiocyanate in acetonitrile and a base catalyst at reflux conditions. Precipitate obtained after cooling was recrystallized using appropriate solvents. Obtained compounds were phenyl isothiocyanates or naphthyl isothiocyanates attached to primary amine not secondary amine of robenidine analogues as shown in Scheme 1. Structural features and physical properties of target compounds **BI** (**1-25**) are shown in Table 1. The structures of the synthesized compounds were elucidated by ^{1}H NMR, ^{13}C NMR, HRMS and FTIR and confirmed by X-ray structure determination. ^{1}H NMR and ^{13}C NMR spectra of the synthesized compounds are provided as supplementary materials. The IR spectra of target compounds **BI (1-25)** exhibited characteristic peaks at 3310-3420 cm^{-1} and 1505-1720 cm^{-1} corresponding to N-H and imine stretching frequency, respectively. The proton NMR of synthesized compounds shown characteristics chemical shifts in the downfield region of the spectra corresponding to the N-H groups. In all compounds, a singlet around 13.08–14.16 ppm corresponding to the N-H was observed. When present in the structure of synthesized compounds, methyl or methoxy groups are observed in the region between 2.33 to 3.85 ppm. Noteworthy, when some of these compounds were dissolved in dimethyl sulfoxide-d_6 for the ^{1}H NMR and ^{13}C NMR analysis they exhibited thiol–thione tautomerism [31,32]. In that case, deuterated chloroform was used as solvent. One of the factors that affects the tautomeric equilibrium is solvent [33]. The ^{13}C NMR exhibited peak around 177.2-178.4 corresponding to the (C=S) and aromatic carbons were screened around 120.3 and 149.3 ppm. Single crystal X-ray data of compound **BI-19** further confirms the structure of the synthesized compounds.

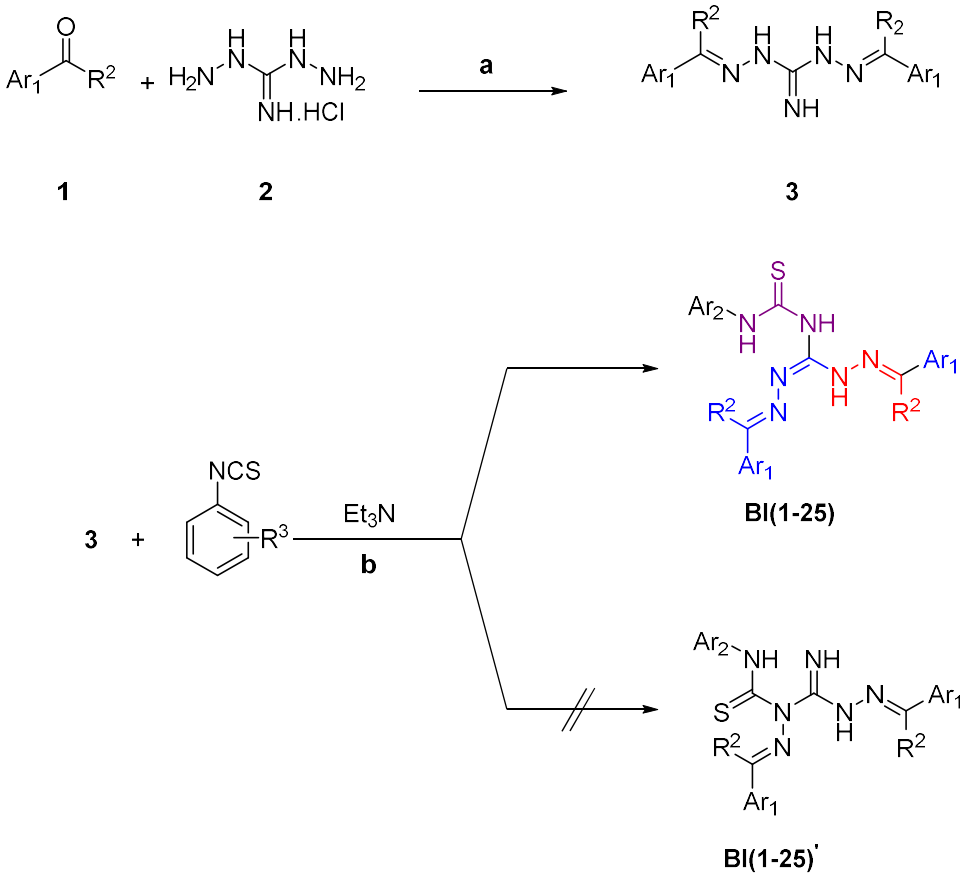

Scheme 1. Synthesis of target compounds **BI (1-25)**, Reagents and Conditions: (a) Ethanol, reflux, 8 h. (b) Acetonitrile, Et_3N, reflux, 16 h.

Table 1. Structural features and physical properties of synthesized compounds **BI (1-25)**.

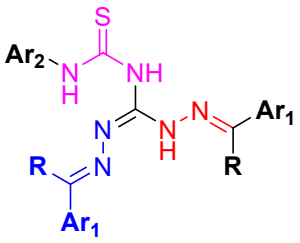

Compounds	R	Ar_1	Ar_2	Yield%	Mp (°C)	Molecular weight

BI-1	CH_3	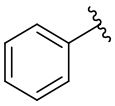	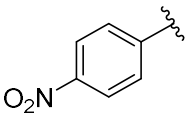	81	209-211	473
BI-2	CH_3	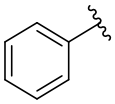	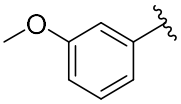	62	142-144	458
BI-3	CH_3	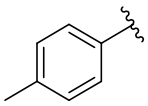	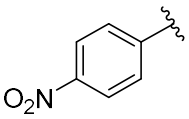	84	215-217	501
BI-4	CH_3	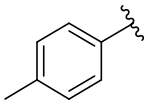	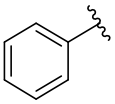	75	164-166	456
BI-5	CH_3	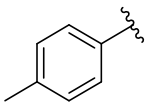	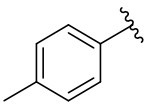	72	170-172	470
BI-6	CH_3	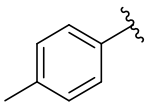	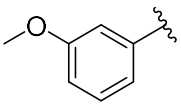	78	156-157	486
BI-7	CH_3	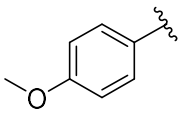	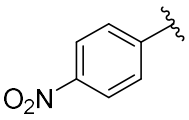	83	214-215	533
BI-8	CH_3	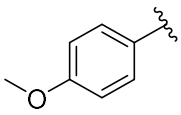	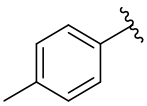	62	149-151	502
BI-9	CH_3	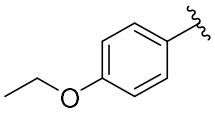	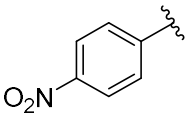	81	192-194	561
BI-10	CH_3	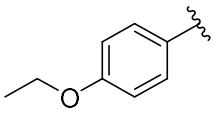	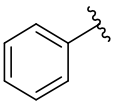	73	152-154	516
BI-11	CH_3	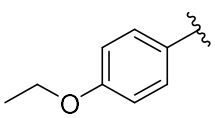	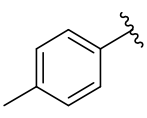	76	138-140	530

BI-12	CH_3	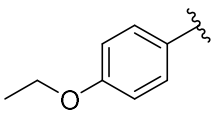	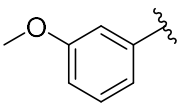	86	163-165	546
BI-13	CH_3	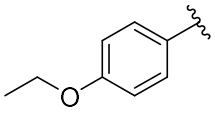	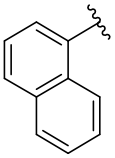	69	164-166	566
BI-14	CH_3	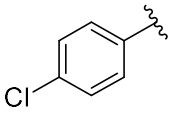	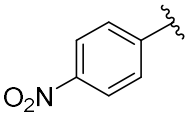	84	212-214	542
BI-15	CH_3	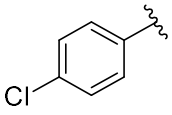	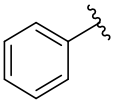	55	155-157	497
BI-16	CH_3	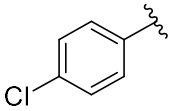	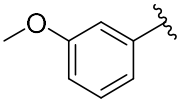	78	158-159	527
BI-17	CH_3	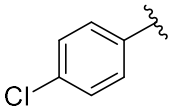	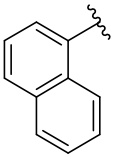	66	189-191	547
BI-18	H	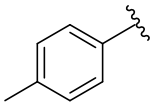	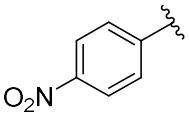	74	158-160	473
BI-19	H	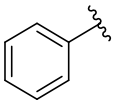	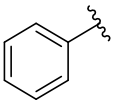	66	149-151	400
BI-20	H	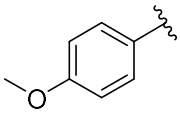	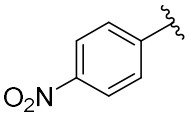	75	182-184	505
BI-21	H	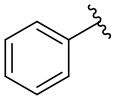	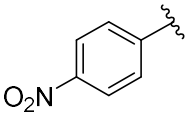	84	202-204	445

BI-22	H	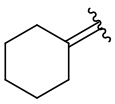	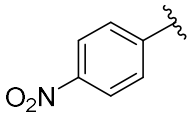	59	195-197	429
BI-23	CH_3	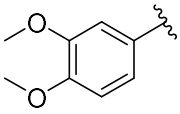	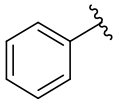	77	208-210	548
BI-24	CH_3	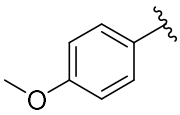	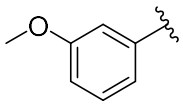	73	172-174	518
BI-25	H	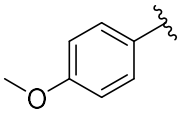	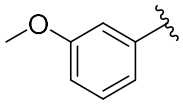	69	161-163	490

2.2. X-ray Structure Determination

The solid-state structure of **BI-19** was unambiguously determined by single-crystal X-ray diffraction analysis in order to get a better understanding of its molecular conformation. **BI-19** crystallizes in the monoclinic crystal system belonging to *P*21/*c* space group, in which the aminoguanidine groups form three N-H···N intramolecular hydrogen bonds (N1···N4 = 2.643 Å, N2···N5 = 2.648 Å, N6···N3 = 2.572 Å) as illustrated in Figure. 4. Two phenyl rings (A/B) lie nearly in the same plane with a negligible tilt angle (θ= 8.96°) while A/C and B/C rings are not coplanar as indicated by dihedral angles of θ = 51.46° and 57.85°, respectively. The C22-S1 bond length is found to be 1.6604(19) Å, which are close to C=S double bond distance in the literature [https://doi.org/10.1016/j.poly.2021.115372]. As shown in Fig. 4 (B and C), the weak CH···S hydrogen bonding interactions (C18···S1 = 3.715 Å) leading a 1D-hydrogen bonded chains and the C-H···π interactions (C3-H3···π, $d_{(H\cdots\pi)}$ = 2.80 Å) running along the *b*-axis contributed to the stability of the solid-state structure.

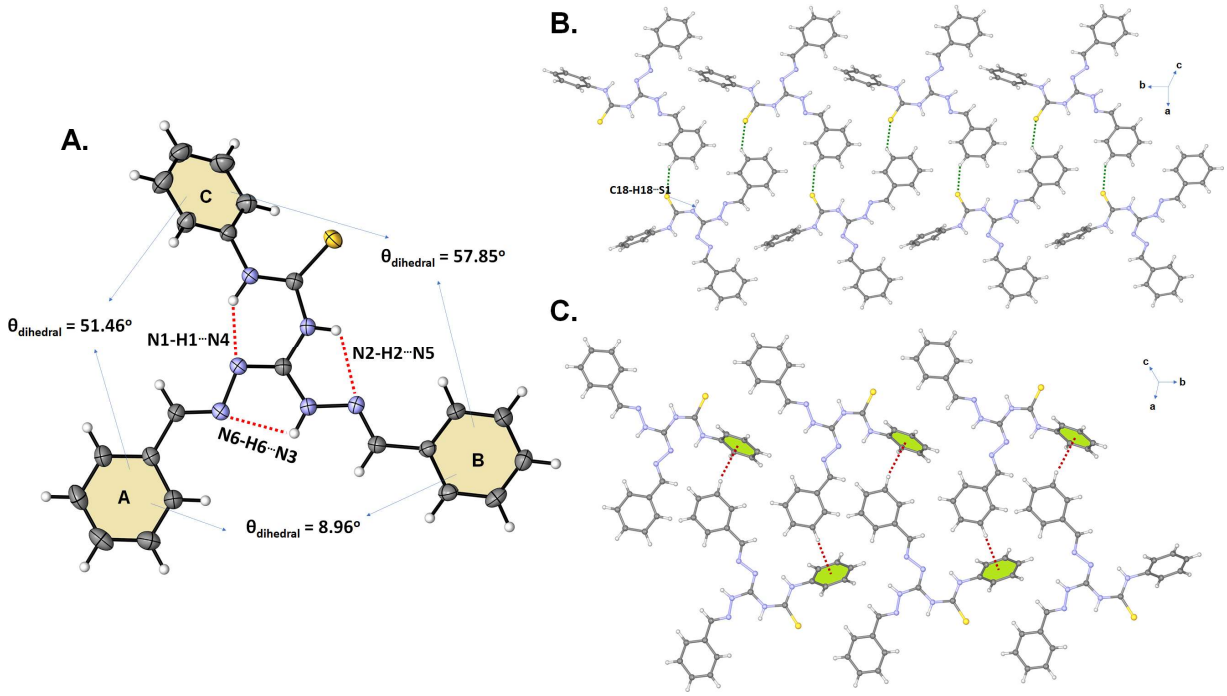

Fig. 4. Crystal structure of **BI-19** with displacement ellipsoids (30% probability level) showing the intramolecular N-H···N hydrogen bonding interactions (N1···N4 = 2.643 Å, N2···N5 = 2.648 Å, N6···N3 = 2.572 Å) and the dihedral angles between the phenyl rings. **B)** and **C)** Perspective view of the C-H···S and C-H···π interactions in the crystal packing. The gray, blue, yellow, and white colored atoms represent C, N, S, and H, respectively.

2.3. Antitubercular and cytotoxicity evaluation

Using the Microplate Alamar Blue Assay (MABA) assay, we evaluated all compounds **BI (1-25)** for antitubercular activity against MTB H37Rv. Four compounds had significant MIC values against MTB H37Rv. Two of them (**BI-16** and **BI-17**) had lower MIC values (1.56 and 0.78 µM, respectively) than the other compounds tested.

It is important to consider the cytotoxicity to host cells, while developing new antitubercular compounds. To determine the cytotoxicity of active compounds against human embryonic kidney (HEK) cells, we used a colorimetric MTT assay. According to the results, our active molecules were also found to be non-toxic (<50%) at a test concentration of 25 µM. Table 2 shows the

cytotoxicity data of the most active derivatives as well as the MIC_{50} (minimum inhibitory concentration that inhibits 5% of the MTB strains).

Table 2. MIC_{50} ± SD values (μM, n=3) of the selected compounds against MTB H37Rv and cytotoxicity data.

Compound	MIC (μM)	Cytotoxicity [a]
BI-1	>100	---
BI-2	>100	
BI-3	>100	
BI-4	100	
BI-5	>100	
BI-6	>100	
BI-7	>100	
BI-8	>100	
BI-9	>100	
BI-10	**12.5**	
BI-11	>100	
BI-12	>100	
BI-13	**6.25**	
BI-14	>100	
BI-15	>100	
BI-16	**1.56 ± 0.92**	**19.14**
BI-17	**0.78 ± 0.25**	**41.31**
BI-18	>100	
BI-19	>100	
BI-20	>100	
BI-21	>100	
BI-22	>100	
BI-23	>100	
BI-24	>100	

BI-25	>100
INH	0.07 ± 0.02

[a] Cytotoxicity is reported as % inhibition determined at 25 µM concentration of test compounds against human embryonic kidney (HEK) cells.

2.4. InhA inhibition assay

The inhibitory activity of compounds **BI-16** and **BI-17** was evaluated according to our previous protocols [35]. Assays were performed using 2-*trans*-dodecenoyl-CoA as substrate at 50 µM of each tested compound. Biaryl ether triclosan (TCL), a known inhibitor of InhA, was used as a positive control [36]. Both compounds showed moderate inhibitory activity against InhA enzyme. (Table 3)

Table 3. Enzyme inhibition values for **BI-16** and **BI-17** derivatives. Results are expressed as a percentage of InhA inhibition.

Compound	% inhibition at 50 µM
BI-16	30
BI-17	24
TCL	98

2.5 Computational Studies

Computer-aided drug discovery/design (CADD) approaches have played a vital role in the development of new therapeutically relevant compounds for more than three decades. CADD has the capacity to boost the hit rate of new medicinal compounds since it uses a far more focused search than traditional high throughput screening and combinatorial chemistry. Interactions between biomolecules are essential for all biological processes. Experimentation and computer simulation and analysis are the one of most important scientific tools for understanding these processes and developing compounds that can be employed as bioactive chemicals to alter and regulate them.

Computational docking is a widely utilized method for studying protein-ligand interactions and identifying new potential therapeutic candidates. A known crystallographic structure of a pharmaceutical enzyme is usually the starting point. Docking is used to predict the binding conformation and free energy of small molecules to the target. Docking of small molecule compounds into a receptor's binding site is an important aspect of structure-based drug design. In order to further analyze the protein-ligand interactions at physiological conditions top-docking poses of ligands were used in MD simulations.

The 4 active hit compounds (**BI-10**, **BI-13**, **BI-16**, and **BI-17**) were subjected to *in silico* calculations, in this study. The molecular docking method can be used to show how a small molecule interacts with a protein, which can aid in describing the behavior of small particles at the target protein's binding site and clarifying crucial biochemical processes. A suitable docking technique can be used to determine the probable binding modes and binding free energy of receptor-ligand complexes. To determine the InhA inhibition potential of these compounds, we used induced fit docking (IFD) and molecular dynamics (MD) simulations. We identified four compounds as possible InhA inhibitors based on the knowledge gained from this work. We run 200-ns MD simulations of the proposed four compounds in order to get structural understanding and confirm the stability of the protein:ligand complex. The change in binding free energies (i.e., MM/GBSA) over time was examined for the four investigated compounds. The computational results are given in Table 4.

Table 4. 2D structure, docking scores in IFD and average MM/GBSA values of four hit compounds.

Compounds	**2D Structure**	**IFD Score (kcal/mol)**	**Average MM/GBSA (kcal/mol)**
BI-10	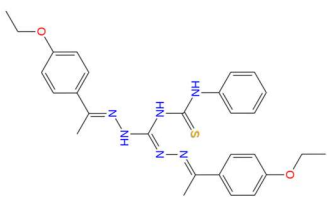	-13.38	-57.21±5.52

BI-13	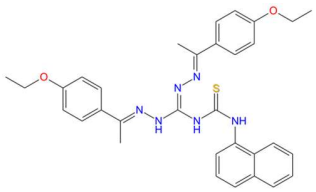	-12.86	-74.88±10.26
BI-16	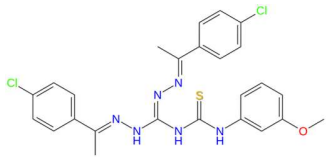	-11.54	-68.94±8.31
BI-17	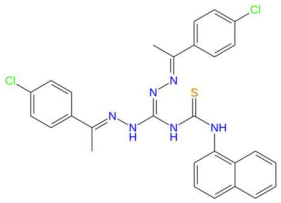	-12.61	-78.61±4.96

The active participation of NADH as a cofactor, which contributes robust contact with substrates through H-bonding involvement from its ribose hydroxyl moiety, is a binding property shared by all InhA inhibitors. Furthermore, Lys165 of InhA contributes to the binding mechanism through hydrogen bonding with the hydroxyl oxygen of the NAD ribose. This residue made a significant

contribution to the cofactor's stability. As a result, the presence of NAD during a study could have a significant impact not only on the ligand interaction but also on the hits occupancy size, which could influence ligand orientation. Furthermore, the majority of identified InhA inhibitors form a permanent hydrogen bond with the backbone hydroxyl group of the main chain Tyr158, which inhibits the activity of the enoyl-acyl carrier protein reductase [34].

2.5.1. Induced fit docking studies

In this study, Glide and Prime modules were used to perform an IFD calculations on the four selected hit compounds in order to estimate their probable binding conformations. The high negative values of the IFD scores indicated that the inhibitors had a high predicted binding affinity for 4TZK (Table 4). Figure 5 depicts the docking position of **BI-17** in the binding pocket of 4TZK.

The highly conserved Gly96, Phe97, Tyr158, Met161 and Met199 residues were found to have favorable hydrophobic interactions. **BI-17** compound was surrounded by Met155, Ala157, Met199 and Ile215, within 4.0 Å suitable for van der Waal's contacts.

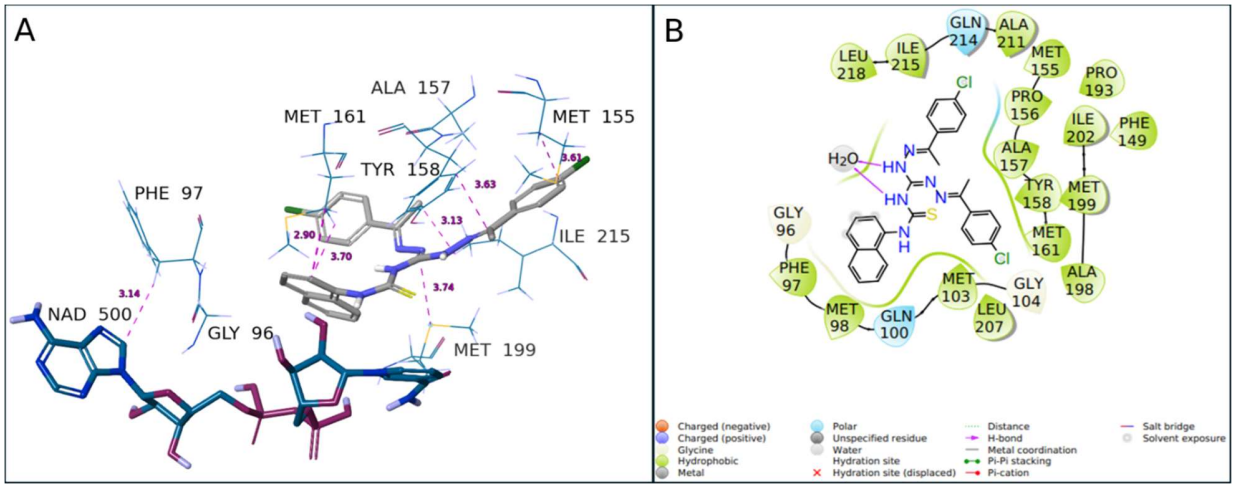

Fig. 5. Top-docking pose of **BI-17** in the binding pocket of InhA (PDB-ID: 4TZK). Figure represents the 3D (A) and 2D (B) interaction of **BI-17**.

2.5.2. Molecular Dynamics (MD) Simulations

To investigate the structural requirements for InhA inhibitory action and obtain a better understanding of the enzyme dynamic behavior, the induced fit docking-simulated structural models of the four selected compounds were used as the starting structures for 200-ns MD simulations. The representative 3D ligand interaction diagrams of the most active ligands **BI-17** and **BI-16** are shown in Figure 6. Binding mode of **BI-17** in the active site of InhA and ligand interaction diagram throughout 200 ns molecular dynamics simulations are depicted in Figure 7.

The top panel of Figure 7 shows the overall number of distinct protein-ligand interactions during the simulations, whereas the bottom panel shows the residue interactions with the ligand in a time-dependent manner. The phenyl ring with Cl atom of **BI-17** compound constructed π-π stacking interaction with Tyr158 of InhA. (Figure 7). **BI-17** also formed other important hydrophobic interactions with Tyr158, Lys165, Ile202 and Ile215. Throughout the simulation period, hydrophobic interactions were found to have a larger influence than other interactions.

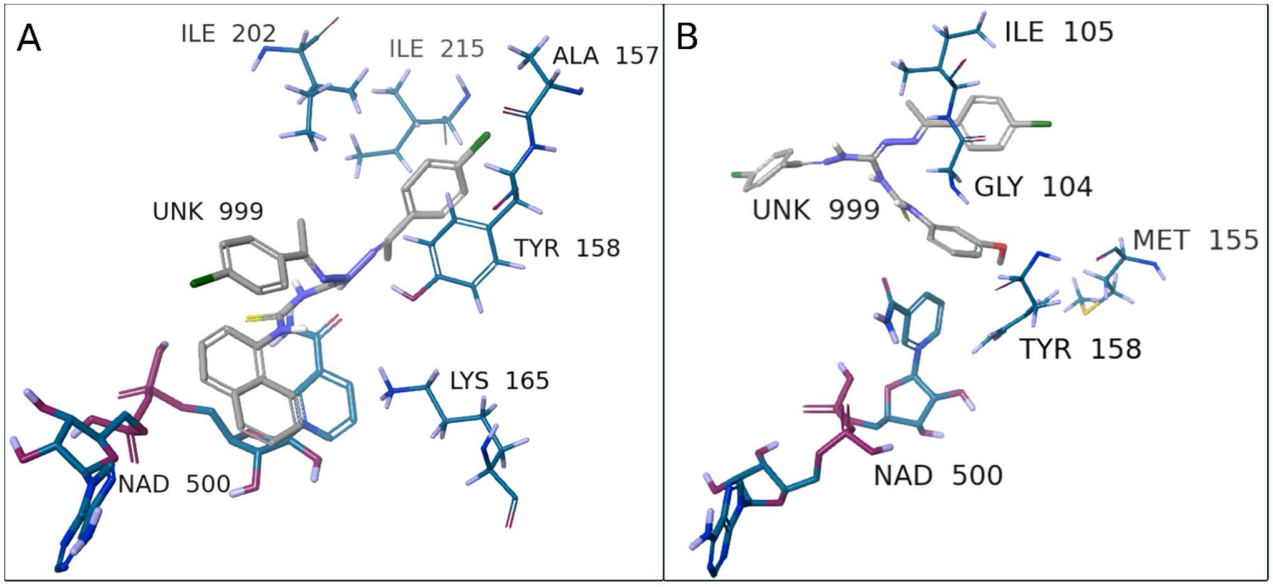

Fig. 6. . 3D interaction diagram of **BI-17** (A) and **BI-16** (B) within the active site of InhA.

BI-16 interactions with the InhA active site were also investigated. (Figure 8) **BI-16** compound has created hydrogen bonding interactions with Met98, Gln100 and Met103 at the active site, as well as hydrophobic contacts with Tyr158, Ile202, Leu207, Ile215 and Leu218. It has been observed that it causes an increase in activity the changing of the $-OCH_3$ group at the phenyl ring of **BI-16** compound to naphthyl at the **BI-17** compound. On the other hand, while the **BI-17** was surrounded by Ala157, Tyr158, and Lys165, Ile202 and Ile215, the **BI-16** was surrounded by

Gly104, Ile105, Met155 and Tyr158. The average binding free energies (MM/GBSA) of compounds **BI-16** and **BI-17** for InhA were found as −68.94 kcal/mol and −78.61 kcal/mol, respectively. These compounds were also determined to be the most effective inhibitor against InhA among the new synthesized compounds (MIC= 6.25 and 3.12 µM, respectively).

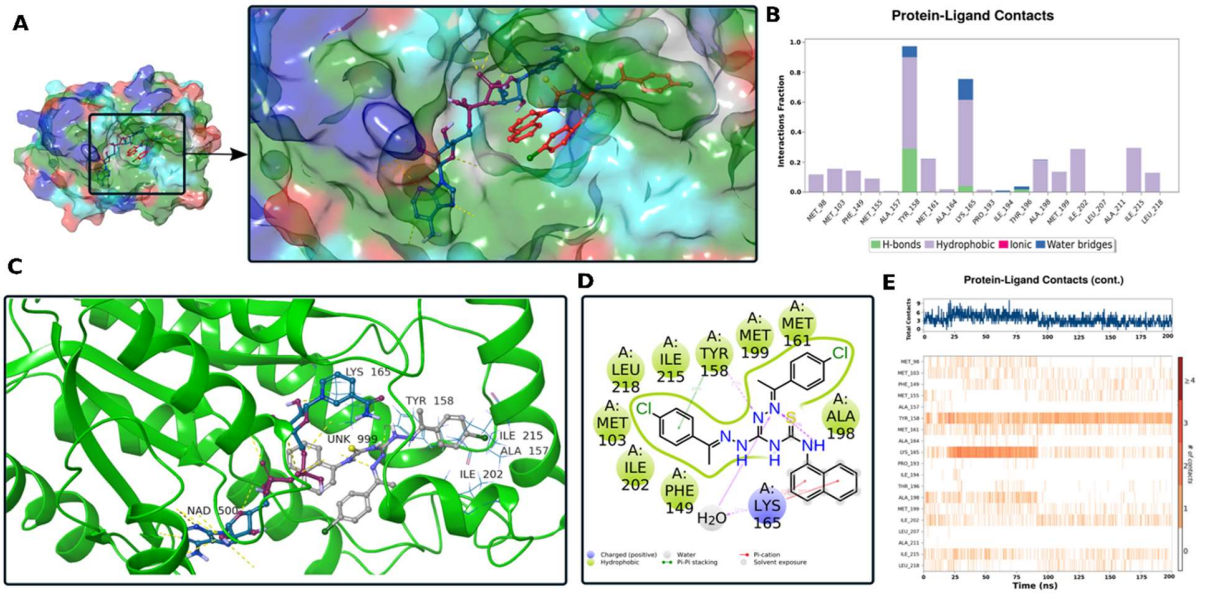

Fig. 7. (A) Representation of **BI-17** binding mode at the InhA surface (B) **BI-17** ligand interaction diagram based on 200 ns molecular dynamics simulations. (C) **BI-17** binding mode in the InhA active site pocket. The protein is represented by ribbons, whereas the ligand is represented by sticks. (D) 2D ligand interactions with InhA protein amino acid residues. (E) Change of protein–ligand contacts throughout the MD simulations for **BI-17.**

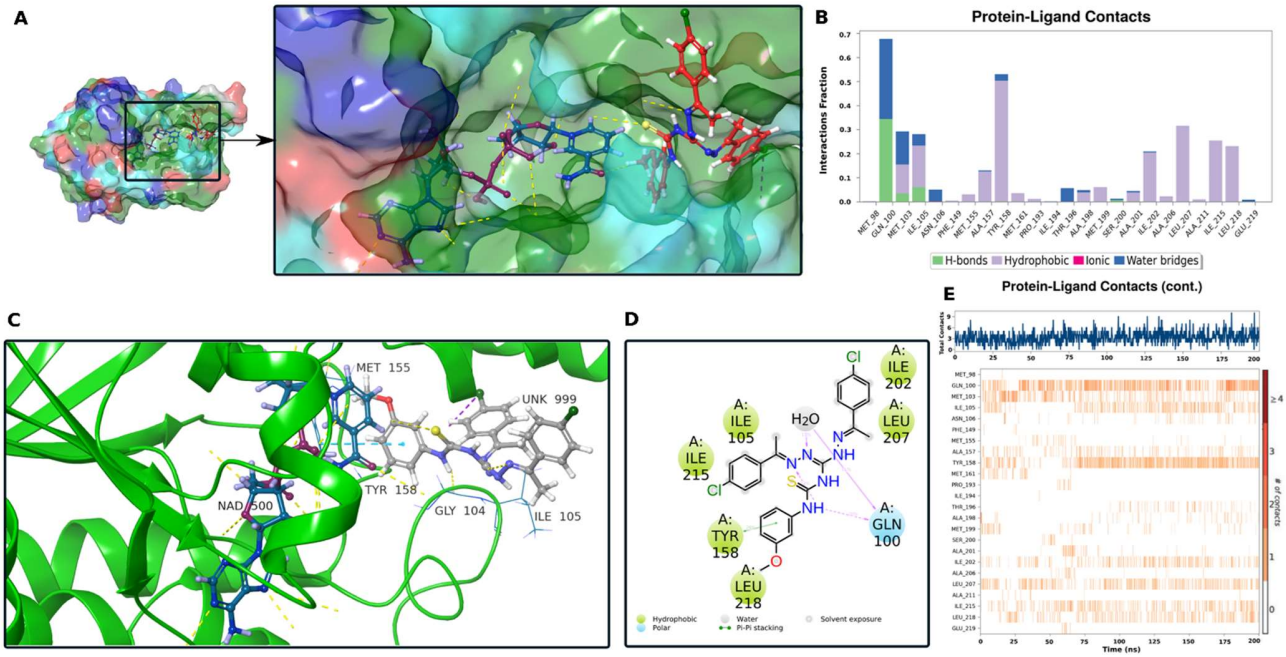

Fig. 8. (A) Representation of **BI-16**'s binding mode at the InhA surface (B) BI-16 ligand interaction diagram based on 200 ns molecular dynamics simulations. (C) BI-16 binding mode in the InhA active site pocket. The protein is represented by ribbons, whereas the ligand is represented by sticks. (D) MD simulations of 2D ligand interactions with InhA protein amino acid residues. (E) Change of protein–ligand contacts throughout the MD simulations for **BI-16**.

Root mean square deviations (RMSDs) of the protein backbone, Cα, and heavy atoms of MD trajectories were determined to investigate the dynamic stability of the four complexes with the hit compounds (Figure 9). The RMSD-time graphs revealed that all the systems exhibit smaller structural changes compared to starting structure. According to the graphs, **BI-16** has the greatest increase in RMSD during the simulation. The maximum RMSD was roughly 3.0 Å, and all atom MD simulations of complex systems were structurally stable after 60 ns. In addition to the protein RMSDS, ligand RMSDs were also investigated. The RMSD of a ligand when the protein–ligand complex is originally aligned on the protein's backbone atoms as a reference state is shown in 'LigFitProt' RMSDs. The RMSD graphs of the studied compounds in LigFitProt are shown in Figure 9, B.

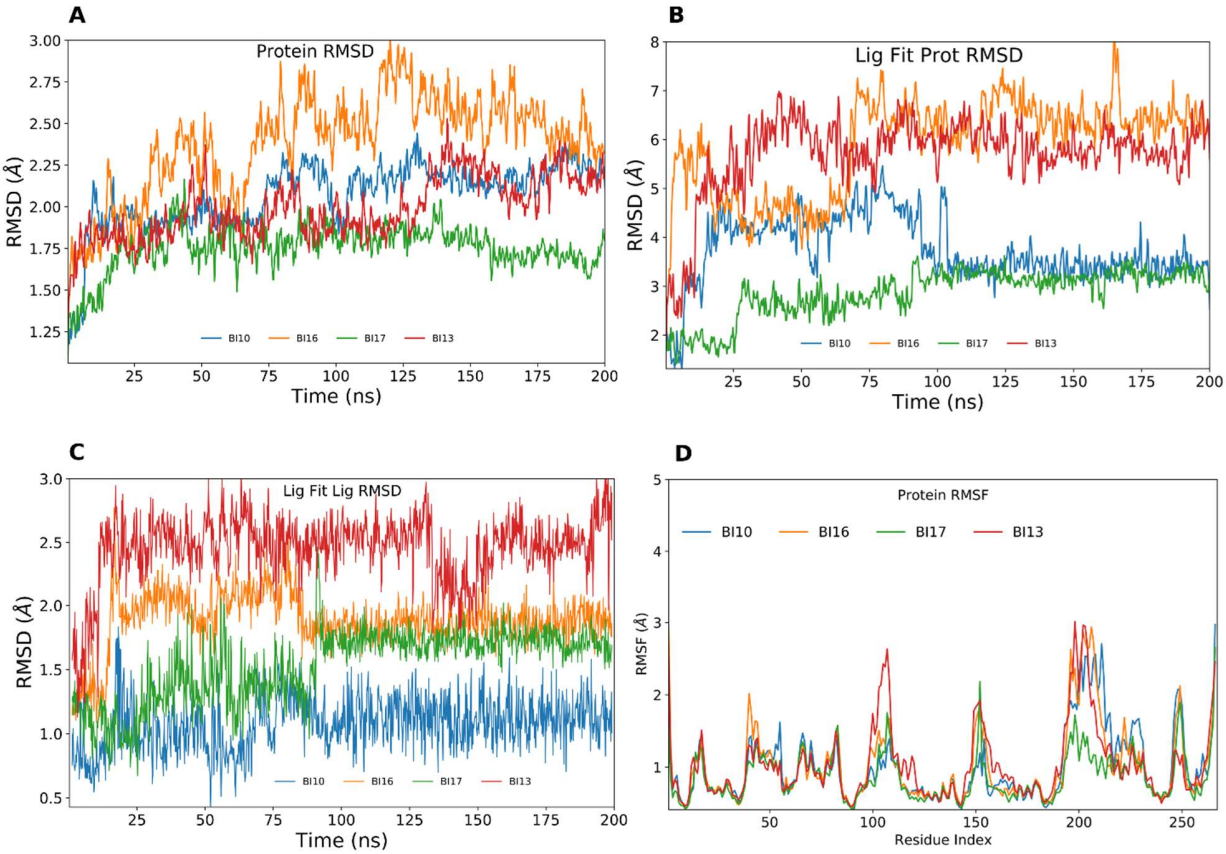

Fig. 9. MD simulations of the complexes formed between InhA and the four hit compounds. (A) RMSD graph of InhA Cα atoms across 200 ns MD simulations. (B) LigFitProt RMSD graph. (C) LigFitLig RMSD graph. (D) RMSF graphs.

The majority of the compounds showed significant changes upon binding to the InhA active site. The results of LigFitProt revealed that **BI-17** has exceptionally low RMSD values (Figure 9, B). In Figure 9, C, the structural motions of the ligands were analyzed using LigFitLig RMSD. All the compounds investigated had average LigFitLig RMSDs of less than 3.0 Å, indicating that the structural motions of the compounds studied do not vary considerably. During the simulations, root mean square fluctuations (RMSF) of the backbone atoms of each residue in the complex were investigated (Figure 9, D). High RMSF values imply highly mobile sections, whereas low RMSF values represent rigid parts of the studied structure. Compound **BI-13** has larger variations around residues 110 and 200. Residues between 190 and 220 have higher fluctuations in the other compounds except **BI-17**.

2.5.3. Binding free energies (MM/GBSA) of the hit compounds

The complexes were submitted to Prime module to calculate binding free energy using the MM/GBSA approach to quantitatively analyze the binding free energies of the four compounds to the 4TZK target. The OPLS-2005 force field was used throughout the calculation. Frames were collected at 10 ps intervals from the MD trajectories of each complex. Table 4 summarizes the findings. Figure 10 depicts the evolution of the MM/GBSA scores of the four compounds throughout the duration of the 200-ns MD simulations. **BI-17** had greater ΔG values (in absolute values) than the other compounds.

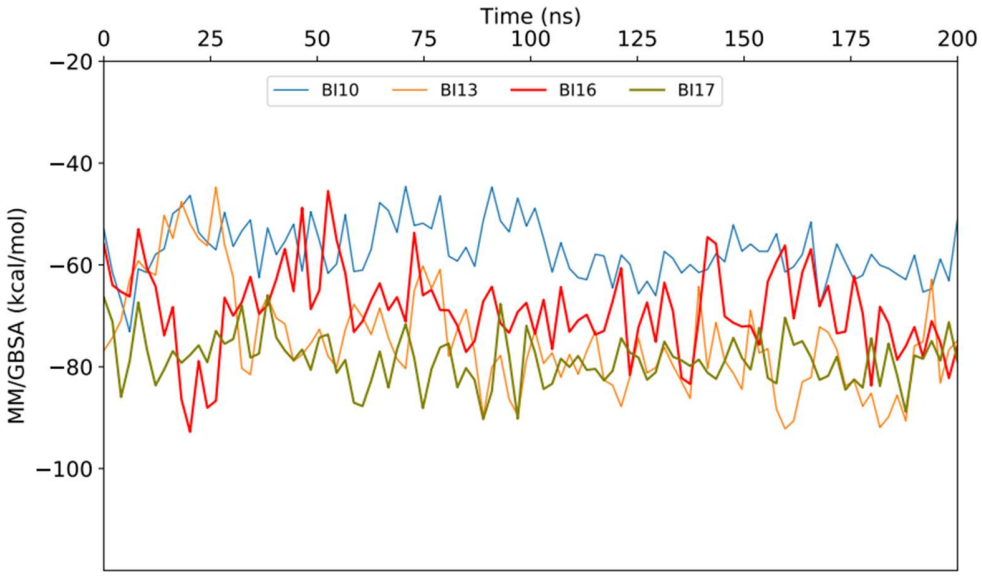

Fig. 10. MM/GBSA free energy analysis for binding of the four investigated four compounds to the InhA binding pocket during MD simulations (MM/GBSA binding energy values in kcal/mol).

3. Conclusion

Since tuberculosis claims a large number of lives around the world, finding new drugs with novel structures and mechanisms of action is critical. Thus, we present a series of thiourea derivatives bearing aminoguanidine moiety as anti-tuberculosis agents. We synthesized effective inhibitors of MTB growth, and attempted to demonstrate their possible mode of action through InhA inhibition, which catalyzes an essential step in fatty acid biosynthesis of MTB. Among synthesized compounds, **BI-16** and **BI-17** showed moderate inhibitory activity against InhA enzyme. Altogether, our data can serve as a template for designing future agents against MTB for the successful clinical control of the disease.

4. Experimental

4.1 Chemistry

4.1.1 Material and methods

All materials were obtained from commercial sources and used without purification unless otherwise stated. Thin layer Chromatography (TLC) with fluorescent indicator visualizable at 254nm and 365 nm was used to determine reaction time and purity of products. Melting points were determined using open glass capillaries and were uncorrected. Infrared (IR) spectra were obtained via ATR diamond in range 4000-600cm^{-1}. ^{1}H NMR (400 MHz) spectra and ^{13}C NMR (100 MHz) spectra were recorded on a Bruker AM 400 MHz NMR spectrometer with $CDCl_3$ or DMSO-d_6 as the solvent. Coupling constants, J, are reported in hertz (Hz). MS spectra were carried out on an LC/MS High-Resolution Time of Flight (TOF) Agilent 1200/6530 instrument at the Atatürk University-East Anatolian High Technology Research and Application Center (DAYTAM).

General Procedure for the synthesis of robenidine analogues **3**.

These compounds were synthesized according to modified literature procedure [9]. Benzaldehydes or acetophenones (**1**) (0.11 mmol) and 1,3 diaminoguanidine hydrochloride (**2**) (0.05 mmol) in 10 mL ethanol were refluxed for. The suspension was neutralized with excess of 2 N KOH.

General Procedure for the synthesis of the target compounds **BI(1-25)**.

To a refluxed solution of 2,2'-bis(4-chlorobenzylidene)carbonimidic dihydrazide (1 mmol.), triethylamine (1.10 mmol) in acetonitrile (6.0 mL) was added phenyl isothiocyanate or naphthyl isothiocyanate (1.10 mmol). The reaction was heated at reflux for 6-8 h (monitored by TLC) and, after cooling, the resulting white precipitate was collected, and recrystallized with appropriate solvents to afford the **BI(1-25)** in good yields (55-86%).

*N-((4-nitrophenyl)carbamothioyl)-N'-(1-phenylethylidene)-2-(1-phenylethylidene)hydrazine-1-carbohydrazonamide (***BI1***) Yield 81%. Mp 209-211 ℃. IR (ATR) 3316.3, 2832.1, 1557.3, 1494.0, 1439.7, 1392.3, 1324.4, 1105.9. ^{1}H NMR (400 MHz, DMSO-d_6) δ 14.08 (s, 1H, NH), 10.66 (s, 1H, NH), 9.96 (s, 1H, NH), 8.46 (d, J = 9.3 Hz, 2H, Ar-H), 8.27 (d, J = 8.7 Hz, 1H, Ar-H), 8.00 (d, J = 9.1 Hz, 2H, Ar-H), 7.87 (d, J = 7.2 Hz, 3H, Ar-H), 7.76 (d, J = 7.2 Hz, 1H, Ar-H), 7.66 (d, J = 8.7 Hz, 1H, Ar-H), 7.38 – 7.21 (m, 4H, Ar-H), 7.18 (d, J = 7.3 Hz, 1H, Ar-H), 2.40 (s, 3H, CH_3),*

2.38 (s, 5H, CH_3). ^{13}C NMR (101 MHz, $CDCl_3$) δ 177.32 C=S, 158.90, 149.57, 144.52, 140.19, 129.40, 129.34, 126.41, 126.17, 124.53, 122.73, 30.94 CH_3, 21.36 CH_3. HRMS (EI): $[M+H]^+$, found 474.17. $C_{24}H_{23}N_7O_2S$ requires 474.16. *High resolution mass spectra : it is fours digits after the dot and not two !!! It should be changed for all the compounds*

*N-((3-methoxyphenyl)carbamothioyl)-N'-(1-phenylethylidene)-2-(1-phenylethylidene)hydrazine-1-carbohydrazonamide (***BI2***) Yield 62%. Mp 142-144. IR (ATR) 3365.4, 2830.7, 1560.4, 1484.7, 1400.4, 1279.9, 1154.8, 1240.7, 1172.6, 1090.2, 827.92, 748.0. ^1H NMR (400 MHz, DMSO-d_6) δ 13.51 (s, 1H, NH), 9.76 (s, 1H, NH), 9.31 (s, 1H, NH), 7.86 (d, J = 7.6 Hz, 3H, Ar-H), 7.72 (d, J = 7.6 Hz, 2H, Ar-H), 7.57 – 7.46 (m, 1H, Ar-H), 7.40 – 7.18 (m, 7H, Ar-H), 6.92 – 6.75 (m, 1H, Ar-H), 3.78 (s, 3H, CH_3), 2.41 (s, 3H, O-CH_3), 2.35 (s, 3H, O-CH_3). ^{13}C NMR (101 MHz, $CDCl_3$) δ 177.05 C=S, 159.85, 158.71, 149.76, 129.79, 129.50, 128.66, 128.57, 126.47, 126.26, 115.89, 112.01, 109.32, 55.42 O-CH_3, 15.48 CH_3, 13.31 CH_3. HRMS (EI): $[M+H]^+$, found 459.19. $C_{25}H_{26}N_6OS$ requires 459.18.*

*N-((4-nitrophenyl)carbamothioyl)-N'-(1-(p-tolyl)ethylidene)-2-(1-(p-tolyl)ethylidene)hydrazine-1-carbohydrazonamide (***BI3***) Yield 84%. Mp 215-217 ℃. IR (ATR) 0000.0, 3277.7, 2811.8, 1571.3, 1500.4, 1437.3, 1401.1, 1322.5, 1298.7, 1242.5, 1171.1, 1139.3, 1104.8, 833.8. ^1H NMR (400 MHz, DMSO-d_6) δ 14.16 (s, 1H, NH), 10.69 (s, 1H, NH), 9.94 (s, 1H, NH), 8.47 (d, J = 9.8 Hz, 1H, Ar-H), 8.28 (d, J = 8.2 Hz, 1H, Ar-H), 8.06 – 7.97 (m, 2H, Ar-H), 7.88 (d, J = 6.0 Hz, 2H, Ar-H), 7.76 (d, J = 7.2 Hz, 2H, Ar-H), 7.31 (d, J = 1.4 Hz, 2H, Ar-H), 7.18 (d, J = 7.6 Hz, 2H, Ar-H), 2.41 (s, 3H, CH_3), 2.38 (s, 3H, CH_3), 2.31 (s, 3H, CH_3), 2.27 (s, 3H, CH_3). ^{13}C NMR (101 MHz, $CDCl_3$) δ 177.29 (C=S), 158.99, 149.55, 144.59, 140.30, 129.41, 126.46, 123.72 (d, J = 164.1 Hz), 122.90, 21.39 CH_3, 15.60 CH_3, 13.38 CH_3. HRMS (EI): $[M+H]^+$, found 502.20. $C_{26}H_{27}N_7O_2S$ requires 502.19.*

*N-(phenylcarbamothioyl)-N'-(1-(p-tolyl)ethylidene)-2-(1-(p-tolyl)ethylidene)hydrazine-1-carbohydrazonamide (***BI4***) Yield 75 ℃. Mp 165-167. IR (ATR) 3354.8, 2830.6, 1614.8, 1493.4, 1393.7, 1249.2, 11.69.7, 1097.8, 812.19. ^1H NMR (400 MHz, DMSO-d_6) δ 13.48 (s, 1H, NH), 9.77 (s, 1H, NH), 9.31 (s, 1H, NH), 7.93 – 7.82 (m, 4H, Ar-H), 7.75 (dd, J = 21.5, 7.7 Hz, 2H, Ar-H), 7.52 – 7.40 (m, 2H, Ar-H), 7.40 – 7.22 (m, 4H, Ar-H), 2.38 (s, 6H, CH_3), 2.35 (s, 6H, CH_3). ^{13}C NMR (101 MHz, $CDCl_3$) δ 177.42 C=S, 158.62, 149.70, 141.38, 139.98, 131.50, 129.36, 128.80,*

126.41, 125.46, 124.01, 21.35 CH_3, 15.46 CH_3, 13.18 CH_3. HRMS (EI): $[M+H]^+$, found 457.21. $C_{26}H_{28}N_6S$ requires 457.21.

*N'-(1-(p-tolyl)ethylidene)-2-(1-(p-tolyl)ethylidene)-N-(p-tolylcarbamothioyl)hydrazine-1-carbohydrazonamide (***BI5***) Yield 72 %. Mp 170-172 °C. IR (ATR) 3374.7, 2909.5, 1592.9, 1504.9, 1398.1, 1247.7, 1167.4, 1096.1, 1059.1, 808.99. ^1H NMR (400 MHz, DMSO-d_6) δ 13.39 (s, 1H, NH), 9.74 (s, 1H, NH), 9.26 (s, 1H, NH), 7.85 (d, J = 7.7 Hz, 2H, Ar-H), 7.71 (d, J = 8.0 Hz, 2H, Ar-H), 7.63 (d, J = 8.0 Hz, 2H, Ar-H), 7.27 (dd, J = 15.7, 7.1 Hz, 6H, Ar-H), 2.38 (s, 3H, CH_3) , 2.35 (s, 3H, CH_3) , 2.34 (s, 3H, CH_3) , 2.32 (s, 3H, CH_3). ^{13}C NMR (101 MHz, $CDCl_3$) δ 172.94 C=S, 158.61, 149.74, 136.24, 134.62, 129.40, 126.46, 124.25, 21 CH_3.38 CH_3, 21.14 CH_3, 15.60 CH_3, 13.29 CH_3. HRMS (EI): $[M+H]^+$, found 471.23. $C_{27}H_{30}N_6S$ requires 471.23.*

*N-((3-methoxyphenyl)carbamothioyl)-N'-(1-(p-tolyl)ethylidene)-2-(1-(p-tolyl)ethylidene)hydrazine-1-carbohydrazonamide (***BI6***) Yield 78 %. Mp 176-178 °C. IR (ATR) 3345.2, 2900.6, 1510.6, 1506.7, 1506.7, 1394.9, 1394.9, 1326.0, 1247.3, 1166.8, 1096.7, 1039.1, 814.2. ^1H NMR (400 MHz, DMSO-d_6) δ 13.51 (s, 1H, NH), 9.76 (s, 1H, NH), 9.31 (s, 1H, NH), 7.86 (d, J = 7.6 Hz, 2H, Ar-H), 7.72 (d, J = 7.6 Hz, 2H, Ar-H), 7.52 (s, 1H, Ar-H), 7.30 (dd, J = 15.7, 8.6 Hz, 6H, Ar-H), 6.95 – 6.80 (m, 1H, Ar-H), 3.78 (s, 3H, O-CH3), 2.41 (s, 3H, CH3), 2.39 (s, 3H, CH3), 2.35 (s, 6H, CH3).^{13}C NMR (101 MHz, $CDCl_3$) δ 177.11 C=S, 162.01, 159.85, 158.63, 149.69, 139.86, 139.05, 129.82, 129.47, 129.36, 129.29, 129.05, 126.40, 115.98, 112.08, 109.40, 55.42 OCH_3, 21.36 CH_3, 15.47 CH_3, 13.21 CH_3. HRMS (EI): $[M+H]^+$, found 487.23. $C_{27}H_{30}N_6OS$ requires 487.22.*

N'-(1-(4-methoxyphenyl)ethylidene)-2-(1-(4-methoxyphenyl)ethylidene)-N-((4-nitrophenyl)carbamothioyl)hydrazine-1-carbohydrazonamide (BI7) Yield 84 %. Mp 214-216 °C. IR (ATR) 3366.0, 2875.7, 1573.9, 1509.7, 1396.9, 1245.3, 1207.6,1037.0, 921.7. ^1H NMR (400 MHz, DMSO-d_6) δ 14.07 (s, 1H, NH), 10.64 (s, 1H, NH), 10.11 (s, 1H, NH), 8.47 (d, J = 8.8 Hz, 2H, Ar-H), 7.98 (dd, J = 25.8, 8.4 Hz, 4H, Ar-H), 7.06 (dd, J = 7.0, 3.0 Hz, 3H, Ar-H), 3.84 (s, 6H, O-CH_3), 2.40 (s, 6H, CH_3). ^{13}C NMR (101 MHz, DMSO-d_6) δ 176.43 (C=S), 161.01, 159.86, 158.11, 151.05, 149.74, 139.82, 130.92, 130.11, 128.68, 128.06, 115.59, 114.50, 114.23, 111.82, 109.22, 55.73 (d, J = 6.8 Hz) OCH_3, 15.11 (CH_3), 14.13 (CH_3). HRMS (EI): $[M+H]^+$, found 534.19. $C_{26}H_{27}N_7O_4S$ requires 534.18.

*N'-(1-(4-methoxyphenyl)ethylidene)-2-(1-(4-methoxyphenyl)ethylidene)-N-(p-tolylcarbamothioyl)hydrazine-1-carbohydrazonamide (***BI8***) Yield 62%. Mp 149-151. IR (ATR) 3349.2, 2831.6, 1603.0, 1564.7, 1501.2, 1397.6, 1314.9, 1248.6, 1167.8, 1094.8, 1035.6, 814.8.* ^{1}*H NMR (400 MHz, DMSO-*d_6*) δ 13.42 (s, 1H, NH), 9.70 (s, 1H, NH), 9.26 (s, 1H, NH), 7.92 (d, J = 7.8 Hz, 2H, Ar-H), 7.78 (d, J = 8.8 Hz, 2H, Ar-H), 7.63 (d, J = 7.5 Hz, 2H, Ar-H), 7.24 (d, J = 7.6 Hz, 2H, Ar-H), 7.02 (dd, J = 18.3, 8.3 Hz, 4H, Ar-H), 3.81 (s, 6H, O-*CH_3*), 2.38 (s, 6H,* CH_3*).* ^{13}*C NMR (101 MHz, DMSO-*d_6*) δ 176.66 C=S, 161.02, 160.97, 158.09, 151.08, 149.78, 136.19, 135.76, 129.69, 128.67, 128.06, 123.78, 114.52, 114.24, 55.77, 55.71 O-* CH_3*, 21.04, 15.05* CH_3*, 14.16* CH_3*. HRMS (EI): [M+H]*$^{+}$*, found 503.22.* $C_{27}H_{30}N_6O_2S$ *requires 503.22.*

*N'-(1-(4-ethoxyphenyl)ethylidene)-2-(1-(4-ethoxyphenyl)ethylidene)-N-((4-nitrophenyl)carbamothioyl)hydrazine-1-carbohydrazonamide (***BI9***) Yield 81%. Mp 192-194. IR (ATR) 3339.7, 3253.6, 2831.6, 1557.2, 1502.2, 1436.2, 1392.5, 1297.5, 1105.3, 922.07. 1H NMR (400 MHz, DMSO-*d_6*) δ 14.06 (s, 1H, NH), 10.60 (s, 1H, NH), 9.90 (s, 1H, NH), 8.46 (d, J = 7.6 Hz, 2H, Ar-H), 7.99 (d, J = 7.4 Hz, 2H, Ar-H), 7.94 – 7.76 (m, 4H, Ar-H), 6.93 (dd, J = 22.3, 13.4 Hz, 4H, Ar-H), 4.15 – 4.03 (m, 4H, O-CH2), 2.35 (s, 6H, CH3), 1.75 – 1.11 (m, 6H, CH3). 13C NMR (101 MHz,* $CDCl_3$*) δ 177.33 C=S, 160.47, 160.40, 158.36, 149.36, 148.18, 144.54, 144.46, 130.58, 129.15, 127.88, 127.63, 124.56, 122.70, 114.51, 114.40, 63.62 O-CH2, 15.35 CH3, 14.80 CH3, 13.18 CH3. HRMS (EI): [M+H]*$^{+}$*, found 562.22.* $C_{28}H_{31}N_7O_4S$ *requires 562.22.*

*N'-(1-(4-ethoxyphenyl)ethylidene)-2-(1-(4-ethoxyphenyl)ethylidene)-N-(phenylcarbamothioyl)hydrazine-1-carbohydrazonamide (***BI10***) Yield 73%. Mp 152-154. IR (ATR) 0000.0, 2973.9, 1598.6, 1508.2, 1390.2, 1301.4, 1242.7, 1172.0, 1043.0, 918.24.* ^{1}*H NMR (400 MHz, DMSO-*d_6*) δ 13.53 (s, 1H, NH), 9.73 (s, 1H, NH), 9.32 (s, 1H, NH), 7.92 (dd, J = 8.6, 3.2 Hz, 3H, Ar-H), 7.77 (d, J = 8.8 Hz, 3H, Ar-H), 7.44 (t, J = 7.8 Hz, 2H, Ar-H), 7.36 – 7.24 (m, 1H, Ar-H), 7.10 – 6.93 (m, 5H, Ar-H), 4.09 (dd, J = 8.4, 5.3 Hz, 4H, O-*CH_2*), 2.38 (s, 6H,* CH_3*), 1.52 – 1.04 (m, 6H,* CH_3*).* ^{13}*C NMR (101 MHz,* $CDCl_3$*) δ 177.32 C=S, 160.31, 158.05, 149.46, 147.61, 138.66, 130.85, 128.80, 128.12, 127.84, 127.62, 126.09, 123.86, 114.45, 114.37, 63.59 O-*CH_2*, 15.17* CH_3*, 14.81* CH_3*, 13.05* CH_3*. HRMS (EI): [M+H]*$^{+}$*, found 517.24.* $C_{28}H_{32}N_6O_2S$ *requires 517.23.*

*N'-(1-(4-ethoxyphenyl)ethylidene)-2-(1-(4-ethoxyphenyl)ethylidene)-N-(p-tolylcarbamothioyl)hydrazine-1-carbohydrazonamide (***BI11***) Yield 76%. Mp 138-140 ℃. IR (ATR)*

3339.7, 2975.3, 1603.6, 1504.9, 1391.1, 1308.9, 1242.7, 1170.4, 1093.7, 1041.6, 919.1. ^{1}H NMR (400 MHz, DMSO-d_6) δ 13.44 (s, 1H, NH), 9.71 (s, 1H, NH), 9.27 (s, 1H, NH), 7.91 (d, J = 6.2 Hz, 2H, Ar-H), 7.76 (d, J = 8.7 Hz, 2H, Ar-H), 7.63 (d, J = 8.0 Hz, 2H, Ar-H), 7.24 (d, J = 7.6 Hz, 2H, Ar-H), 7.00 (dd, J = 19.3, 8.5 Hz, 4H, Ar-H), 4.08 (dd, J = 6.6, 4.7 Hz, 4H, O-CH_2), 2.38 (s, 3H, CH_3), 2.36 (s, 1H, CH_3), 2.32 (s, 3H, CH_3), 1.56 – 0.99 (m, 6H, CH_3). ^{13}C NMR (101 MHz, $CDCl_3$) δ 177.49 C=S, 164.80, 158.08, 149.48, 129.69, 129.38, 128.34, 124.29, 114.92, 114.45, 114.08, 63.64, 63.57 O-CH_2, 21.13 CH_3, 14.79 CH_3. HRMS (EI): $[M+H]^+$, found 531.25. $C_{29}H_{34}N_6O_2S$ requires 531.25.

*N'-(1-(4-ethoxyphenyl)ethylidene)-2-(1-(4-ethoxyphenyl)ethylidene)-N-((3-methoxyphenyl)carbamothioyl)hydrazine-1-carbohydrazonamide (***BI12***) Yield 86%. Mp 163-165. IR (ATR) 3366.0, 2875.7, 1573.9, 1509.8, 1396.9, 1245.3, 1207.6, 1037.0, 921.6. ^{1}H NMR (400 MHz, DMSO-d_6) δ 13.55 (s, 1H, NH), 9.71 (s, 1H, NH), 9.30 (s, 1H, NH), 7.91 (d, J = 8.7 Hz, 2H, Ar-H), 7.76 (d, J = 8.7 Hz, 2H, Ar-H), 7.52 (s, 1H, Ar-H), 7.33 (d, J = 7.1 Hz, 2H, Ar-H), 7.00 (dd, J = 18.9, 8.7 Hz, 4H, Ar-H), 4.08 (dd, J = 9.0, 4.7 Hz, 4H, O-CH_2), 3.77 (s, 3H, O-CH_2), 2.39 (s, 3H, CH_3), 2.37 (s, 3H, CH_3), 1.35 (t, J = 6.7 Hz, 6H, CH_3). ^{13}C NMR (101 MHz, $CDCl_3$) δ 176.88 C=S, 160.30, 160.24, 159.82, 157.88, 149.39, 147.55, 139.82, 130.79, 129.45, 129.30, 127.82, 127.59, 115.64, 114.43, 114.35, 111.78, 109.05, 63.57 O-CH_2, 55.39 O-CH_3, 14.82 CH_3, 12.98 CH_3. HRMS (EI): $[M+H]^+$, found 547.25. $C_{29}H_{34}N_6O_3S$ requires 547.24.*

*N'-(1-(4-ethoxyphenyl)ethylidene)-2-(1-(4-ethoxyphenyl)ethylidene)-N-(naphthalen-1-ylcarbamothioyl)hydrazine-1-carbohydrazonamide (***BI13***) Yield 69%. Mp 164-166 ℃. IR (ATR) 3378.6, 2970.6, 1568.1, 1505.9, 1392.0, 1244.3, 177.9, 1042.4, 827.10. ^{1}H NMR (400 MHz, DMSO-d_6) δ 13.59 (s, 1H, NH), 9.80 (s, 1H, NH), 9.50 (s, 1H, NH), 8.01 (dd, J = 16.4, 9.0 Hz, 4H, Ar-H), 7.94 (d, J = 8.3 Hz, 1H, Ar-H), 7.89 (d, J = 8.8 Hz, 2H, Ar-H), 7.82 (dd, J = 13.6, 8.0 Hz, 2H- Ar-H), 7.61 (dd, J = 9.7, 5.8 Hz, 2H- Ar-H), 7.04 (d, J = 8.9 Hz, 2H, Ar-H), 6.96 (d, J = 8.8 Hz, 2H), Ar-H, 4.08 (dd, J = 9.5, 4.9 Hz, 4H, O-CH_2), 2.42 (s, 3H, CH_3), 2.36 (s, 3H, CH_3), 1.42 – 1.30 (m, 6H, CH_3). ^{13}C NMR (101 MHz, $CDCl_3$) δ 179.42 (C=S), 160.78, 160.74, 160.49, 160.36, 154.38, 134.27, 129.20, 128.44, 128.13, 127.76, 126.66, 126.34, 125.36, 63.65 (CH_2), 16.11(CH_3), 14.76 (CH_3). HRMS (EI): $[M+H]^+$, found 567.25. $C_{32}H_{34}N_6O_2S$ requires 567.25.*

*N'-(1-(4-chlorophenyl)ethylidene)-2-(1-(4-chlorophenyl)ethylidene)-N-((4-nitrophenyl)carbamothioyl)hydrazine-1-carbohydrazonamide (***BI14***) Yield 84%. Mp 212-214 ℃.*

IR (ATR) 3344.3, 3269.2, 2773.5, 1566.9, 1489.0, 1435.5, 1398.3, 1362.8, 1322.9, 1242.9, 1175.4, 967.53. ^{1}H NMR (400 MHz, DMSO-d_6) δ 14.15 (s, 1H, NH), 10.74 (s, 1H, NH), 10.24 (s, 1H, NH), 8.11 – 7.86 (m, 8H, Ar-H), 7.55 (d, J = 7.8 Hz, 2H, Ar-H), 7.42 (d, J = 8.6 Hz, 2H, Ar-H), 2.43 (s, 3H, CH_3), 2.29 (s, 3H, CH_3). ^{13}C NMR (101 MHz, $CDCl_3$) δ 177.32 (C=S), 158.90, 149.57, 144.52, 140.19, 129.40, 129.34, 126.41, 126.17, 124.53, 122.73, 15.53 (CH_3), 13.27 (CH_3). HRMS (EI): $[M+H]^+$, found 543.10. $C_{24}H_{21}Cl_2N_7O_2S$ requires 543.09.

*N'-(1-(4-chlorophenyl)ethylidene)-2-(1-(4-chlorophenyl)ethylidene)-N-(phenylcarbamothioyl)hydrazine-1-carbohydrazonamide (***BI15***) Yield 55%. Mp 155-157 °C. IR (ATR) 3362.7, 2830.0, 1585.9, 1489.7, 1299.4, 1246.3, 1165.8, 1108.7, 1027.0, 822.43. ^{1}H NMR (400 MHz, DMSO-d_6) δ 13.41 (s, 1H, NH), 9.86 (s, 1H, NH), 9.33 (s, 1H, NH), 7.99 (d, J = 7.6 Hz, 2H, Ar-H), 7.85 (d, J = 8.1 Hz, 2H, Ar-H), 7.77 (d, J = 7.7 Hz, 2H, Ar-H), 7.53 (dd, J = 19.7, 8.4 Hz, 4H, Ar-H), 7.48 – 7.41 (m, 2H, Ar-H), 7.31 – 7.21 (m, 1H, Ar-H), 2.41 (s, 6H, CH_3). ^{13}C NMR (101 MHz, $CDCl_3$) δ 177.29 C=S, 157.83, 157.36, 149.66, 135.90, 129.26, 128.91, 128.88, 128.78, 127.69, 127.49, 126.33, 123.92, 15.38 CH_3, 13.19 CH_3. HRMS (EI): $[M+H]^+$, found 498.11. $C_{24}H_{22}Cl_2N_6S$ requires 498.10.*

*N'-(1-(4-chlorophenyl)ethylidene)-2-(1-(4-chlorophenyl)ethylidene)-N-((3-methoxyphenyl)carbamothioyl)hydrazine-1-carbohydrazonamide (***BI16***) Yield 78%. Mp 158-160 °C. IR (ATR) 3342.0, 3263.7, 2974.1, 2887.7, 1617.7, 1586.2, 1508.3, 1487.7, 1435.7, 1167.8.^{1}H NMR (400 MHz, DMSO-d_6) δ 13.47 (s, 1H, NH), 9.92 (s, 1H, NH), 9.38 (s, 1H, NH), 8.00 (d, J = 7.5 Hz, 4H, Ar-H), 7.86 (d, J = 7.0 Hz, 1Har-H), 7.54 (dd, J = 21.3, 8.6 Hz, 4H, Ar-H), 7.45 (d, J = 8.6 Hz, 2Har-H), 7.34 (d, J = 8.8 Hz, 1H, Ar-H), 3.78 (s, 3H, O-CH_3), 2.43 (s, 3H, CH_3), 2.33 (s, 3H, CH_3). ^{13}C NMR (101 MHz, $CDCl_3$) δ 159.83 C=S, 157.71, 149.61, 129.50, 128.85, 127.92, 115.86, 109.38, 55.41 O-CH_3, 16.28 CH_3. HRMS (EI): $[M+H]^+$, found 527.12. $C_{25}H_{24}Cl_2N_6OS$ requires 527.11.*

*N'-(1-(4-chlorophenyl)ethylidene)-2-(1-(4-chlorophenyl)ethylidene)-N-(naphthalen-1-ylcarbamothioyl)hydrazine-1-carbohydrazonamide (***BI17***) Yield 66%. Mp 189-191 °C. IR (ATR) 3404.7, 2997.4, 1906.4, 1672.3, 1542.3, 1489.1, 1397.9, 1308.2, 1266.6, 1139.2, 1003.9, 959.7. ^{1}H NMR (400 MHz, DMSO-d_6) δ 13.59 (s, 1H, NH), 9.80 (s, 1H, NH), 9.50 (s, 1H, NH), 8.09 – 7.92 (m, 4H, Ar-H), 7.91 – 7.76 (m, 4H, Ar-H), 7.61 (dd, J = 9.7, 5.8 Hz, 2H, Ar-H), 7.04 (d, J = 8.9 Hz, 2H, Ar-H), 6.96 (d, J = 8.8 Hz, 3H, Ar-H), 2.42 (s, 3H, CH_3), 2.36 (s, 3H, CH_3). ^{13}C NMR*

(101 MHz, $CDCl_3$) δ 177.02 (C=S), 157.94, 150.62 , 149.38, 149.03, 148.78, 147.00, 138.59, 131.20, 129.65, 128.78, 126.02, 123.52, 120.06, 119.37, 110.50 (d, J = 7.2 Hz), 108.56, 108.28, 15.05 (CH_3), 12.65 (CH_3). HRMS (EI): $[M+H]^+$, found 547.12. $C_{28}H_{24}Cl_2N_6S$ requires 547.12.

*N',2-bis(4-methylbenzylidene)-N-((4-nitrophenyl)carbamothioyl)hydrazine-1-carbohydrazonamide (***BI18***) Yield 74%. Mp 158-160 °C. IR (ATR) 3333.3 2900.2, 1619.7, 1573.9, 1505.2, 1488.0, 1359.1, 1321.0, 1257.1, 1105.2, 950.0. ^1H NMR (400 MHz, DMSO-d_6) δ 13.53 (s, 1H, NH), 11.33 (s, 1H, NH), 10.57 (s, 1H, NH), 8.68 – 8.41 (m, 2H, Ar-H), 8.31 (dd, J = 24.2, 8.4 Hz, 2H, Ar-H), 8.15 (d, J = 7.9 Hz, 2H, Ar-H), 7.86 (s, 2H, N=CH), 7.72 – 7.50 (m, 2H, Ar-H), 7.31 (d, J = 7.7 Hz, 4H, Ar-H), 2.37 (s, 10H, CH_3). ^{13}C NMR (101 MHz, $CDCl_3$) δ 177.18 C=S, 154.74, 149.55, 144.59, 144.47, 144.03, 141.27, 141.25, 131.39, 129.99, 129.71, 129.59, 127.84, 127.32, 124.53, 122.64, 21.60 CH_3. HRMS (EI): $[M+H]^+$, found 474.17.$C_{24}H_{23}N_7O_2S$ requires 474.16.*

*N',2-di(benzylidene)-N-(phenylcarbamothioyl)hydrazine-1-carbohydrazonamide (***BI19***) Yield 84%. Mp 149-151 °C. IR (ATR) 3321.1, 3331.6, 2846.0, 1620.3, 1590.7, 1557.9, 1510.8, 1427.9, 1381.0, 1181.5, 1019.5, 942.5. ^1H NMR (400 MHz, DMSO-d_6) δ 13.48 (s, 1H, NH), 11.34 (s, 1H, NH), 9.28 (s, 1H, NH), 8.51 (s, 2H, N=CH), 7.98 (d, J = 7.8 Hz, 2H, Ar-H), 7.78 (d, J = 8.6 Hz, 2H, Ar-H), 7.72 (d, J = 7.7 Hz, 1H, Ar-H), 7.59 – 7.40 (m, 9H, Ar-H), 7.33 – 7.23 (m, 1H, Ar-H). ^{13}C NMR (101 MHz, $CDCl_3$) δ 177.37 (s), 154.49 (s), 143.48 (s), 140.50 (s), 132.81 (s), 131.51 (s), 130.68 (s), 129.78 (s), 129.60 (s), 129.15 (d, J = 9.6 Hz), 129.04 (d, J = 12.5 Hz), 128.98 (s), 128.86 (s), 128.09 – 127.61 (m), 127.39 (d, J = 12.1 Hz), 126.57 (s), 124.38 (s). HRMS (EI): $[M+H]^+$, found 401.15. $C_{22}H_{20}N_6S$ requires 401.15.*

*N',2-bis(4-methoxybenzylidene)-N-((4-nitrophenyl)carbamothioyl)hydrazine-1-carbohydrazonamide (***BI20***) Yield 75%. Mp 182-184 °C. IR (ATR) 3347.7, 3268.8, 2807.1, 1614.3, 1597.5, 1510.7, 1323.1, 1172.2, 1125.6, 1008.9, 971,43. ^1H NMR (400 MHz, DMSO-d_6) δ 13.56 (s, 1H, NH), 11.29 (s, 1H, NH), 10.49 (s, 1H, NH), 8.48 (s, 1H, N=CH), 8.34 (d, J = 9.2 Hz, 2H, Ar-H), 8.23 (s, 1H, N=CH), 8.13 (d, J = 9.2 Hz, 1H, Ar-H), 7.82 (dd, J = 80.5, 23.0 Hz, 4H, Ar-H), 7.05 (d, J = 8.5 Hz, 4H, Ar-H), 3.83 (s, 6H, O-CH_3). ^{13}C NMR (101 MHz, $CDCl_3$) δ 177.11 C=S, 161.70, 154.14 (d, J = 6.2 Hz), 144.48, 143.58, 129.49, 128.91, 128.34, 125.42, 124.47, 122.51, 114.41 (s), 114.32, 55.42 OCH_3. HRMS (EI): $[M+H]^+$, found 506.16. $C_{24}H_{23}N_7O_4S$ requires 506.15.*

*N',2-di(benzylidene)-N-((4-nitrophenyl)carbamothioyl)hydrazine-1-carbohydrazonamide (***BI21***) Yield 84%. Mp 202-204 °C. IR (ATR) 3373.5, 3325.3, 2982.1,1563.4, 1557.3, 1494.0, 1392.3, 1324.4, 1162.9, 1105.9, 910.6.* ^{1}*H NMR (400 MHz, CDCl*$_3$*) δ 13.86 (s, 1H, NH), 9.48 (s, 1H, NH), 9.28 (s, 1H, NH), 8.29 (s, 3H, N=CH, Ar-H), 8.11 (s, 3H, Ar-H), 7.81 (s, 4H, Ar-H), 7.48 (s, 6H, Ar-H).* ^{13}*C NMR (101 MHz, CDCl*$_3$*) δ 177.21 C=S, 154.85, 149.70, 144.72, 134.07, 132.64, 130.90, 129.03, 128.89, 127.92, 127.42, 124.56, 122.78. HRMS (EI): [M+H]*$^{+}$*, found 446.14.* $C_{22}H_{19}N_7O_2S$ *requires 446.13.*

*N',2-dicyclohexylidene-N-((4-nitrophenyl)carbamothioyl)hydrazine-1-carbohydrazonamide (***BI22***) Yield 59%. Mp 195-197 °C. IR (ATR) 3342.0, 2919.1, 2840.7, 1620.3, 1582.4, 1493.2, 1503.3, 1417.4, 1391.4, 1256.2, 1222.4, 1082.0, 892.1.* ^{1}*H NMR (400 MHz, DMSO-d*$_6$*) δ 13.72 (s, 1H, NH), 10.46 (s, 2H, NH), 10.06 (s, 1H, NH), 8.45 (d, J = 8.9 Hz, 2H, Ar-H), 8.05 (d, J = 8.8 Hz, 2H,Ar-H), 2.43 (d, J = 3.0 Hz, 8H, CH*$_2$*), 1.85 – 1.30 (m, 12H, CH*$_2$*).* ^{13}*C NMR (101 MHz, CDCl*$_3$*) δ 177.52 C=S, 167.57, 149.75, 147.29, 144.80, 125.48, 124.50, 122.63, 116.63, 35.64 CH*$_2$*, 35.22 CH*$_2$*, 26.82 CH*$_2$*, 26.29 CH*$_2$*, 25.89 CH*$_2$*, 25.63 CH*$_2$*, 25.43 CH*$_2$*. HRMS (EI): [M+H]*$^{+}$*, found 430.20.* $C_{20}H_{27}N_7O_2S$ *requires 430.19.*

*N'-(1-(3,4-dimethoxyphenyl)ethylidene)-2-(1-(3,4-dimethoxyphenyl)ethylidene)-N-(phenylcarbamothioyl)hydrazine-1-carbohydrazonamide (***BI23***) Yield 77%. Mp 208-210 °C. IR (ATR) 3342.0, 3237.6, 2830.3, 1612.5, 1587.1, 1509.1, 1426.8, 1326.6, 1254.5, 1141.3, 1108.3, 1028.7, 964.9.*^{1}*H NMR (400 MHz, DMSO-d*$_6$*) δ 13.46 (s, 1H, NH), 9.79 (s, 1H, NH), 9.60 (s, 1H, NH), 7.79 (d, J = 7.6 Hz, 1H, Ar-H), 7.72 (s, 1H, Ar-H), 7.49 – 7.34 (m, 5H, Ar-H), 7.31 – 7.23 (m, 1H, Ar-H), 7.01 (dd, J = 17.5, 8.4 Hz, 2H, Ar-H), 6.93 (d, J = 8.5 Hz, 1H, Ar-H), 3.84 (s, 3H, O-CH*$_3$*), 3.83 (s, 3H, O-CH*$_3$*), 3.79 (s, 3H, O-CH*$_3$*), 3.78 (s, 3H, O-CH*$_3$*), 2.40 (s, 3H, CH*$_3$*).* ^{13}*C NMR (101 MHz, CDCl*$_3$*) δ 177.02 (C=S), 157.94, 150.62, 149.38, 149.03, 148.78, 147.00, 138.59, 131.20, 129.65, 128.78, 126.02, 123.52, 120.06, 119.37, 110.53, 110.46, 108.56, 108.28, 55.97 (OCH*$_3$*), 15.05 (CH*$_3$*), 12.65 (CH*$_3$*). HRMS (EI): [M+H]*$^{+}$*, found 549.22.* $C_{28}H_{32}N_6O_4S$ *requires 549.22.*

*N-((3-methoxyphenyl)carbamothioyl)-N'-(1-(4-methoxyphenyl)ethylidene)-2-(1-(4-methoxyphenyl)ethylidene)hydrazine-1-carbohydrazonamide (***BI24***) Yield 73%. Mp 172-174 °C. IR (ATR) 3335.1, 2924.3, 1615.1, 1565.5, 1490.2, 1329.3, 1251.0, 1043.4, 1024.9, 861.2.* ^{1}*H NMR (400 MHz, DMSO-d*$_6$*) δ 13.54 (s, 1H, NH), 9.69 (s, 1H, NH), 9.34 (s, 1H, NH), 7.92 (d, J = 8.0 Hz,*

2H, Ar-H), 7.77 (d, J = 7.8 Hz, 2H, Ar-H), 7.52 (s, 1H, Ar-H), 7.33 (d, J = 4.9 Hz, 2H, Ar-H), 7.18 – 6.98 (m, 4H, Ar-H), 6.88 – 6.80 (m, 1H, Ar-H), 3.81 (s, J = 13.6 Hz, 6H, O-CH_3), 3.77 (s, 3H, O-CH_3), 2.39 (s, 6H, CH_3). ^{13}C NMR (101 MHz, $CDCl_3$) δ 177.40 C=S, 158.91, 148.62, 144.56, 144.50, 140.18, 135.53, 134.10, 129.41, 129.32, 126.39, 126.14, 124.55, 122.76, 21.34 O-CH_3, 15.49 CH_3, 13.25 CH_3. HRMS (EI): $[M+H]^+$, found 519.22. $C_{25}H_{26}N_6O_3S$ requires 519.21.

*N',2-bis(4-methoxybenzylidene)-N-((3-methoxyphenyl)carbamothioyl)hydrazine-1-carbohydrazonamide (***BI25***) Yield 69%. Mp 161-163. IR (ATR) 3374.7, 2909.5, 1592.9, 1504.9, 1398.1, 1247.7, 1167.4, 1096.1, 1059.1, 808.9. ^1H NMR (400 MHz, DMSO-d_6) δ 13.56 (s, 1H, NH), 11.12 (s, 1H, NH), 9.22 (s, 1H, NH), 8.42 (d, J = 7.3 Hz, 2H, Ar-H), 7.93 (s, 1H, N=CH), 7.91 (s, 1H, N=CH), 7.65 (d, J = 8.4 Hz, 2H, Ar-H), 7.60 (s, 1H, Ar-H), 7.41 – 7.32 (m, 1H, Ar-H), 7.24 (d, J = 7.6 Hz, 1H, Ar-H), 7.07 (d, J = 8.5 Hz, 2H, Ar-H), 7.02 (d, J = 8.6 Hz, 2H, Ar-H), 6.85 (d, J = 7.8 Hz, 1H, Ar-H), 3.82 (s, 6H, O-CH_3), 3.79 (s, 3H, O-CH_3). HRMS (EI): $[M+H]^+$, found 491.19. $C_{25}H_{26}N_6O_3S$ requires 491.18.*

4.2. X-ray diffraction analysis

Single crystal X-ray diffraction data for **BI-19** was performed on a Bruker D8-QUEST three-circle diffractometer with a graphite-monochromatized Mo-Kα X-radiation (λ = 0.71073 Å). Indexing, data collection, data reduction [37] and absorption correction [38] were carried out using APEX2 [39]. Crystal structure (**1**) were solved using SHELXT [40] and then refined by full-matrix least-squares refinements on F^2 using the SHELXL [41] in Olex2 Software Package [42] The aromatic C-bound H atoms were positioned geometrically and refined using a riding mode. The N-H distances were restrained to be 0.86 A from N atom, and their positions were constrained to refine on their parent N atoms with $U_{iso}(H) = 1.2U_{eq}(N)$. Crystal structure validations, geometrical calculations and drawings were performed using Platon [43] and Mercury software [44] Additional crystallographic data with CCDC reference number 2145264 (compound **1**) has been deposited within the Cambridge Crystallographic Data Center *via* www.ccdc.cam.ac.uk/deposit. Crystallographic data and refinement details of the data collection are given in Table 5.

Table 5. Crystal data and structure refinement details for compound **1**. (To Supporting Information)

Compound	**BI-19**

CCDC	2145264
Empirical formula	$C_{18}H_{20}N_4O_3S$
Formula weight/g. mol^{-1}	400.50
Temperature/K	297
Radiation, Wavelength (Å)	MoKα (λ = 0.71073)
Crystal system	Monoclinic
Space group	$P2_1/c$
a/Å	13.6242(6)
b/Å	11.6790(5)
c/Å	13.7610(5)
α/°	90
β/°	109.878(2)
γ/°	90
Volume/Å^3	2059.15(15)
Z	4
ρ_{calcd} (g. cm^{-3})	1.292
μ (mm^{-1})	0.178
***F*(000)**	840
2θ range for data collection (°)	6.012 to 50
h*/*k*/*l	-16 ≤ h ≤ 16, -13 ≤ k ≤ 13, -16 ≤ l ≤ 16
Reflections collected	30201
Independent reflections	3615 [R_{int} = 0.0576, R_{sigma} = 0.0323]
Data/restraints/parameters	3615/0/263
Goodness-of-fit on F^2 (S)	1.038
Final R indices [$I > 2\sigma(I)$]	R_1 = 0.0433, wR_2 = 0.0990
R indices (all data)	R_1 = 0.0747, wR_2 = 0.1099
Largest diff. peak/hole / e Å^{-3}	0.14/-0.25

4.3. Antitubercular activity

Mycobacterium tuberculosis H37Rv (Mtb) was streaked on 7H10+OADC agar plates and incubated at 37 °C. In Sauton's medium, pure colonies from agar plates were grown to mid-log phase. Test compounds were serially diluted using Sauton's medium in 96 well plates. Mtb cultures were then exponentially cultivated and placed about $4x10^5$ CFU/mL in 200 µL each well. Plates were incubated at 37 °C for 1 week before receiving 32.5 µL of a resazurin-tween mixture (8:5 ratio of 0.6 mM Resazurin in 1X PBS to 20% Tween 80) and incubated overnight at 37 °C. The synthesis of fluorescent resorufin aids in the determination of the minimum inhibitory concentration (MIC) of the test compounds [45,46].

4.4. Cytotoxicity screening

The MTT (3-(4,5-dimethylthiazol-2-yl)-2,5-diphenyltetrazolium bromide) test was used to determine the toxicity of the compounds against Human Embryonic Kidney (HEK 293) cell lines. Test compounds (25 µM) were seeded to a sterile 96 well microtiter plate containing 5×10^3 cells and grown at 37°C with 5% CO_2 for 48 hours. Following the incubation period, 10 µL MTT reagent (5 mg/mL) was added to the plate and incubated for an additional 3 hours. The medium was then withdrawn, and each well was filled with 100 µL of DMSO. DMSO dissolves the formazan crystals that have developed in the wells. The absorbance was measured at 580 nm against a blank using a Thermo Scientific Varioskan LUX microplate reader. The cytotoxicity was assessed as a reduction in inhibition in percent [47,48].

4.5. InhA activity inhibition

InhA was purified according to an established protocol [35]. Stock solutions of compounds **BI-16** and **BI-17** were prepared in DMSO. Kinetic assays were performed using *trans*-2-dodecenoyl-coenzyme A (DDCoA) as substrate and His_6-tagged InhA as previously described [35]. Briefly, reactions were performed at 25 °C in an aqueous buffer (30 mM PIPES and 150 mM NaCl pH 6.8, DMSO 5% v/v) containing additionally 250 µM cofactor (NADH), 50 µM substrate (DDCoA) and the tested compounds, each at 50 µM. Reactions were initiated by addition of InhA (100 nM final) and NADH oxidation was followed at 340 nm. The inhibitory activity of each derivative was expressed as the percentage inhibition of InhA activity (initial velocity of the reaction) with respect to the control reaction without inhibitor. All activity assays were performed in duplicate or triplicate when inhibition was observed.

4.6. *In silico* approaches and binding mechanism

4.6.1. Ligand Preparation

At neutral pH, ionization states of compounds were created using EPIK[49]. A maximum of 32 stereoisomers were created for each molecule. An OPLS-2005 (Optimized Potentials for Liquid Simulations) [50] force field was utilized to reduce the energy of each compound with default values.

4.6.2. Preparation of Target Protein

Protein Data Bank (PDB) was used to obtain the crystal structures of as Mycobacterium tuberculosis growth and enoyl acyl carrier protein reductase (InhA) (PDB ID: 4TZK) with a resolution of 1.62 Å. The target protein was prepared before the ligands docked into the active site using the Maestro molecular modeling package's Protein Preparation module. To add missing loops and side chains to the residues, the Maestro's Prime module [51] was utilized. Hydrogen atoms were added to the protein using PROPKA [52] at physiological pH to define correct ionization states of amino acid residues. The protein was relaxed using structural optimization with the OPLS-2005 force field (the 0.3 Å RMSD convergence criterion for heavy atoms was taken into account). In Maestro's receptor-grid generation module, the grid box was formed by selecting the bound ligand center as the workspace ligand's centroid.

4.6.3. Molecular Docking

The Maestro molecular modeling package's Induced-Fit Docking (IFD) module has been widely used flexible docking approach and it is certified as a trustworthy and effective methodology for accounting for ligand and receptor flexibility. The predicted binding affinity of protein/ligand complexes was calculated using the IFD method [53].

4.6.4. Induced Fit Docking (IFD) and Extra Precision (XP) Protocol

IFD and XP were performed using Schrödinger-Maestro V.9.3. Glide/SP (standard precision) docking [54] was initially used for each ligand. The region of 5 Å around the docked ligand (i.e.,

protein-ligand complex) is taken into account for optimization. Eventually, the optimized complex was utilized as the default conditions in redocking.

4.6.5. Molecular Dynamics (MD) Simulations

Molecular Dynamics (MD) simulations was conducted to investigate the structural and dynamical features of docked complex using Desmond V 4.9. [55]. An orthorhombic simple point charge (SPC) water model [56] was created using the system builder panel. To neutralize the system, 8 Na^+ counter ions were added, as well as 150 mM NaCl to maintain the isosmotic salt environment. The refined system was subjected to 200 ns MD simulations (i.e., production run) using the 310 K and 1.013 bar NPT ensemble after minimization and equilibration states (with default relaxation setting). Temperature and pressure were controlled using the Nose-Hoover-Chain thermostat [57] and the Martyna-Tobias-Klein barostat [58]. A time step of 2 fs was used in the simulation, and the energy and structure were recorded and saved in the trajectory every 10 ps.

4.6.6. Calculations of Binding Free Energies of Studies Ligands by Molecular Mechanics Generalized *Born* Surface Area (MM/GBSA) Method

The MM/GBSA method is a well-defined method to calculate the free energy of a small ligand binding to a biological target. The resulting trajectory frames from MD simulations were used in MM/GBSA. In terms of accuracy and computing ability, it sits somewhere between empirical scoring (i.e., molecular docking) and alchemical perturbation techniques. The utilization of a set of structures (snapshots or frames) to account for the protein–ligand complex's conformational flexibility [59] is a significant benefit of the MM/GBSA procedure. It has been discovered that among ligand binding free energy calculation methodologies such as MM/GBSA, thermodynamic integration, and free energy perturbation (FEP), MM/GBSA is the fastest [60]. The MM/GBSA technique is extensively used in free energy calculations, and it yields superior results than docking [61]. The VSGB solvation model, which is a realistic parametrization of the solvation that occurs to the complex in water, was used to determine protein stability. 3.0 Å from the ligand was taken into account [62].

Declaration of competing interest

No potential conflicts of interest were disclosed by the authors.

Acknowledgements

The authors are indebted to the Research Foundation of Erciyes University (Grant No: FYL-2021-11122) for their financial support of this work.

References

[1] G.W. van and Z.M. Baddeley Annabel, Dean Anna, Dias Hannah monica, Falzon Dennis, Floyd Katherine, Garcia Ines, Glaziou Philippe, Hiatt Tom, Law Irwin, Lienhardt Christian, Nguyen Linh, Sismanidis Charalambos, Timimi Hazim, Global Tuberculosis Report 2013 - World Health Organization - Google Books, Who. (2013).

[2] S. Konduri, D. Bhargavi, J. Prashanth, V.S. Krishna, D. Sriram, K.P. Rao, Design and Synthesis of "chloropicolinate Amides and Urea Derivatives" as Novel Inhibitors for Mycobacterium tuberculosis, ACS Omega. 6 (2021) 1657–1667. https://doi.org/10.1021/acsomega.0c05690.

[3] M. Biava, G.C. Porretta, G. Poce, A. De Logu, M. Saddi, R. Meleddu, F. Manetti, E. De Rossi, M. Botta, 1,5-Diphenylpyrrole derivatives as antimycobacterial agents. Probing the influence on antimycobacterial activity of lipophilic substituents at the phenyl rings, J. Med. Chem. 51 (2008) 3644–3648. https://doi.org/10.1021/jm701560p.

[4] A. Campaniço, R. Moreira, F. Lopes, Drug discovery in tuberculosis. New drug targets and antimycobacterial agents, Eur. J. Med. Chem. 150 (2018) 525–545. https://doi.org/10.1016/j.ejmech.2018.03.020.

[5] F. Saczewski, Ł. Balewski, Biological activities of guanidine compounds, Expert Opin. Ther. Pat. 19 (2009) 1417–1448. https://doi.org/10.1517/13543770903216675.

[6] P. Gilbert, L.E. Moore, Cationic antiseptics: Diversity of action under a common epithet, J. Appl. Microbiol. 99 (2005) 703–715. https://doi.org/10.1111/j.1365-2672.2005.02664.x.

[7] P. Broxton, P.M. Woodcock, F. Heatley, P. Gilbert, Interaction of some

polyhexamethylene biguanides and membrane phospholipids in Escherichia coli, J. Appl. Bacteriol. 57 (1984) 115–124. https://doi.org/10.1111/j.1365-2672.1984.tb02363.x.

[8] S.H. Kim, D. Semenya, D. Castagnolo, Antimicrobial drugs bearing guanidine moieties: A review, Eur. J. Med. Chem. 216 (2021) 113293. https://doi.org/10.1016/j.ejmech.2021.113293.

[9] R.J. Abraham, A.J. Stevens, K.A. Young, C. Russell, A. Qvist, M. Khazandi, H.S. Wong, S. Abraham, A.D. Ogunniyi, S.W. Page, R. O'Handley, A. McCluskey, D.J. Trott, Robenidine Analogues as Gram-Positive Antibacterial Agents, J. Med. Chem. 59 (2016) 2126–2138. https://doi.org/10.1021/acs.jmedchem.5b01797.

[10] C.C. Russell, A. Stevens, H. Pi, M. Khazandi, A.D. Ogunniyi, K.A. Young, J.R. Baker, S.N. McCluskey, S.W. Page, D.J. Trott, A. McCluskey, Gram-Positive and Gram-Negative Antibiotic Activity of Asymmetric and Monomeric Robenidine Analogues, ChemMedChem. 13 (2018) 2573–2580. https://doi.org/10.1002/cmdc.201800463.

[11] A. Krollenbrock, Y. Li, J.X. Kelly, M.K. Riscoe, Robenidine Analogues Are Potent Antimalarials in Drug-Resistant Plasmodium falciparum, ACS Infect. Dis. 7 (2021) 1956–1968. https://doi.org/10.1021/acsinfecdis.1c00001.

[12] R. Bairwa, M. Kakwani, N.R. Tawari, J. Lalchandani, M.K. Ray, M.G.R. Rajan, M.S. Degani, Novel molecular hybrids of cinnamic acids and guanylhydrazones as potential antitubercular agents, Bioorganic Med. Chem. Lett. 20 (2010) 1623–1625. https://doi.org/10.1016/j.bmcl.2010.01.031.

[13] V. Velezheva, P. Brennan, P. Ivanov, A. Kornienko, S. Lyubimov, K. Kazarian, B. Nikonenko, K. Majorov, A. Apt, Synthesis and antituberculosis activity of indole-pyridine derived hydrazides, hydrazide-hydrazones, and thiosemicarbazones, Bioorganic Med. Chem. Lett. 26 (2016) 978–985. https://doi.org/10.1016/j.bmcl.2015.12.049.

[14] R.M. Beteck, R. Seldon, A. Jordaan, D.F. Warner, H.C. Hoppe, D. Laming, L.J. Legoabe, S.D. Khanye, Quinolone-isoniazid hybrids: Synthesis and preliminary: In vitro cytotoxicity and anti-tuberculosis evaluation, Medchemcomm. 10 (2019) 326–331. https://doi.org/10.1039/c8md00480c.

[15] Ł. Popiołek, Hydrazide–hydrazones as potential antimicrobial agents: overview of the literature since 2010, Med. Chem. Res. 26 (2017) 287–301. https://doi.org/10.1007/s00044-016-1756-y.

[16] P. Kumar, K. Kadyan, M. Duhan, J. Sindhu, V. Singh, B.S. Saharan, Correction: Design, synthesis, conformational and molecular docking study of some novel acyl hydrazone based molecular hybrids as antimalarial and antimicrobial agents. [Chemistry Central Journal 11, (2017) (115)] DOI: 10.1186/s13065-017-0344-7, Chem. Cent. J. 12 (2018) 1–14. https://doi.org/10.1186/s13065-018-0374-9.

[17] Y.Q. Hu, S. Zhang, F. Zhao, C. Gao, L.S. Feng, Z.S. Lv, Z. Xu, X. Wu, Isoniazid derivatives and their anti-tubercular activity, Eur. J. Med. Chem. 133 (2017) 255–267. https://doi.org/10.1016/j.ejmech.2017.04.002.

[18] F.M.F. Vergara, C.H. d. S. Lima, M. das G.M. d. O. Henriques, A.L.P. Candéa, M.C.S. Lourenço, M. de L. Ferreira, C.R. Kaiser, M.V.N. de Souza, Synthesis and antimycobacterial activity of N′-[(E)-(monosubstituted-benzylidene)]-2-pyrazinecarbohydrazide derivatives, Eur. J. Med. Chem. 44 (2009) 4954–4959. https://doi.org/10.1016/j.ejmech.2009.08.009.

[19] H. Doğan, Ş.D. Doğan, M.G. Gündüz, V.S. Krishna, C. Lherbet, D. Sriram, O. Şahin, E. Sarıpınar, Discovery of hydrazone containing thiadiazoles as Mycobacterium tuberculosis growth and enoyl acyl carrier protein reductase (InhA) inhibitors, Eur. J. Med. Chem. 188 (2020) 112035. https://doi.org/10.1016/j.ejmech.2020.112035.

[20] N.A. Meanwell, Synopsis of some recent tactical application of bioisosteres in drug design, J. Med. Chem. 54 (2011) 2529–2591. https://doi.org/10.1021/jm1013693.

[21] A. Shakeel, Thiourea Derivatives in Drug Design and Medicinal Chemistry: A Short Review, J. Drug Des. Med. Chem. 2 (2016) 10. https://doi.org/10.11648/j.jddmc.20160201.12.

[22] A. Melamud, G.S. Kosmorsky, M.S. Lee, Ocular Ethambutol Toxicity, Mayo Clin. Proc. 78 (2003) 1409–1411. https://doi.org/10.4065/78.11.1409.

[23] A.E. Grzegorzewicz, N. Eynard, A. Quémard, E.J. North, A. Margolis, J.J. Lindenberger,

V. Jones, J. Korduláková, P.J. Brennan, R.E. Lee, D.R. Ronning, M.R. McNeil, M. Jackson, Covalent Modification of the Mycobacterium tuberculosis FAS-II Dehydratase by Isoxyl and Thiacetazone, ACS Infect. Dis. 1 (2016) 91–97. https://doi.org/10.1021/id500032q.

[24] K. Rožman, I. Sosič, R. Fernandez, R.J. Young, A. Mendoza, S. Gobec, L. Encinas, A new 'golden age' for the antitubercular target InhA, Drug Discov. Today. 22 (2017) 492–502. https://doi.org/10.1016/j.drudis.2016.09.009.

[25] M.H. Hazbón, M. Brimacombe, M.B. Del Valle, M. Cavatore, M.I. Guerrero, M. Varma-Basil, H. Billman-Jacobe, C. Lavender, J. Fyfe, L. García-García, C.I. León, M. Bose, F. Chaves, M. Murray, K.D. Eisenach, J. Sifuentes-Osornio, M.D. Cave, A.P. De León, D. Alland, Population genetics study of isoniazid resistance mutations and evolution of multidrug-resistant Mycobacterium tuberculosis, Antimicrob. Agents Chemother. 50 (2006) 2640–2649. https://doi.org/10.1128/AAC.00112-06.

[26] U. Chandra Kumar, S. Mahmood, R. Uday, C. Kumar, IDENTIFICATION OF NEW COMPOUNDS AGAINST ISONIAZID TARGET OF MYCOBACTERIUM TUBERCULOSIS, Pharmacologyonline. 3 (2010) 177–185.

[27] P.S. Shirude, P. Madhavapeddi, M. Naik, K. Murugan, V. Shinde, R. Nandishaiah, J. Bhat, A. Kumar, S. Hameed, G. Holdgate, G. Davies, H. McMiken, N. Hegde, A. Ambady, J. Venkatraman, M. Panda, B. Bandodkar, V.K. Sambandamurthy, J.A. Read, Methyl-thiazoles: A novel mode of inhibition with the potential to develop novel inhibitors targeting InhA in mycobacterium tuberculosis, J. Med. Chem. 56 (2013) 8533–8542. https://doi.org/10.1021/jm4012033.

[28] M.G. Gündüz, S.B. Uğur, F. Güney, C. Özkul, V.S. Krishna, S. Kaya, D. Sriram, Ş.D. Doğan, 1,3-Disubstituted urea derivatives: Synthesis, antimicrobial activity evaluation and in silico studies, Bioorg. Chem. 102 (2020) 104104. https://doi.org/10.1016/j.bioorg.2020.104104.

[29] R.C. Hartkoorn, C. Sala, J. Neres, F. Pojer, S. Magnet, R. Mukherjee, S. Uplekar, S. Boy-Röttger, K.H. Altmann, S.T. Cole, Towards a new tuberculosis drug: Pyridomycin - nature's isoniazid, EMBO Mol. Med. 4 (2012) 1032–1042.

https://doi.org/10.1002/emmm.201201689.

[30] F. Kurzer, K. Douraghi-Zadeh, 822. Heterocyclic compounds from urea derivatives. Part VIII. Addition products of NN′-di(isopropylideneamino)guanidine and isothiocyanate esters, and their cyclisation, J. Chem. Soc. (1965) 4448–4455. https://doi.org/10.1039/JR9650004448.

[31] A. Boshaala, M.A. Said, E.A. Assirey, Z.S. Alborki, A.A. AlObaid, A. Zarrouk, I. Warad, Crystal structure, MEP/DFT/XRD, thione ⇔ thiol tautomerization, thermal, docking, and optical/TD-DFT studies of (E)-methyl 2-(1-phenylethylidene)-hydrazinecarbodithioate ligand, J. Mol. Struct. 1238 (2021) 130461. https://doi.org/10.1016/j.molstruc.2021.130461.

[32] M.D. Davari, H. Bahrami, Z.Z. Haghighi, M. Zahedi, Quantum chemical investigation of intramolecular thione-thiol tautomerism of 1,2,4-triazole-3-thione and its disubstituted derivatives, J. Mol. Model. 16 (2010) 841–855. https://doi.org/10.1007/s00894-009-0585-z.

[33] H. Gökce, N. Öztürk, Ü. Ceylan, Y.B. Alpaslan, G. Alpaslan, Thiol-thione tautomeric analysis, spectroscopic (FT-IR, Laser-Raman, NMR and UV-vis) properties and DFT computations of 5-(3-pyridyl)-4H-1,2,4-triazole-3-thiol molecule, Spectrochim. Acta - Part A Mol. Biomol. Spectrosc. 163 (2016) 170–180. https://doi.org/10.1016/j.saa.2016.03.041.

[34] A. Chollet, L. Maveyraud, C. Lherbet, V. Bernardes-Génisson, An overview on crystal structures of InhA protein: Apo-form, in complex with its natural ligands and inhibitors, Eur. J. Med. Chem. 146 (2018) 318–343. https://doi.org/10.1016/j.ejmech.2018.01.047.

[35] A. Chollet, G. Mori, C. Menendez, F. Rodriguez, I. Fabing, M.R. Pasca, J. Madacki, J. Korduláková, P. Constant, A. Quémard, V. Bernardes-Génisson, C. Lherbet, M. Baltas, Design, synthesis and evaluation of new GEQ derivatives as inhibitors of InhA enzyme and Mycobacterium tuberculosis growth, Eur. J. Med. Chem. 101 (2015) 218–235. https://doi.org/10.1016/j.ejmech.2015.06.035.

[36] M.R. Kuo, H.R. Morbidoni, D. Alland, S.F. Sneddon, B.B. Gourlie, M.M. Staveski, M.

Leonard, J.S. Gregory, A.D. Janjigian, C. Yee, J.M. Musser, B. Kreiswirth, H. Iwamoto, R. Perozzo, W.R. Jacobs, J.C. Sacchettini, D.A. Fidock, Targeting tuberculosis and malaria through inhibition of enoyl reductase. Compound activity and structural data, J. Biol. Chem. 278 (2003) 20851–20859. https://doi.org/10.1074/jbc.M211968200.

[37] SAINT, version 8.34A, Bruker (2013), Bruker AXS Inc., Madison, WI

[38] SADABS, version2014/5, Bruker (2014), Bruker AXS Inc., Madison, WI

[39] APEX2, version 2014.11-0, Bruker (2014), Bruker AXS Inc., Madison, WI

[40] G.M. Sheldrick, SHELXT - Integrated space-group and crystal-structure determination, Acta Crystallogr. Sect. A Found. Crystallogr. 71 (2015) 3–8. https://doi.org/10.1107/S2053273314026370.

[41] G.M. Sheldrick, Crystal structure refinement with SHELXL, Acta Crystallogr. Sect. C Struct. Chem. 71 (2015) 3–8. https://doi.org/10.1107/S2053229614024218.

[42] O. V. Dolomanov, L.J. Bourhis, R.J. Gildea, J.A.K. Howard, H. Puschmann, OLEX2: A complete structure solution, refinement and analysis program, J. Appl. Crystallogr. 42 (2009) 339–341. https://doi.org/10.1107/S0021889808042726.

[43] A.L. Spek, Structure validation in chemical crystallography, Acta Crystallogr. Sect. D Biol. Crystallogr. 65 (2009) 148–155. https://doi.org/10.1107/S090744490804362X.

[44] C.F. MacRae, I. Sovago, S.J. Cottrell, P.T.A. Galek, P. McCabe, E. Pidcock, M. Platings, G.P. Shields, J.S. Stevens, M. Towler, P.A. Wood, Mercury 4.0: From visualization to analysis, design and prediction, J. Appl. Crystallogr. 53 (2020) 226–235. https://doi.org/10.1107/S1600576719014092.

[45] V.S. Krishna, S. Zheng, E.M. Rekha, R. Nallangi, D. V. Sai Prasad, S.E. George, L.W. Guddat, D. Sriram, Design and development of ((4-methoxyphenyl)carbamoyl) (5-(5-nitrothiophen-2-yl)-1,3,4-thiadiazol-2-yl)amide analogues as Mycobacterium tuberculosis ketol-acid reductoisomerase inhibitors, Eur. J. Med. Chem. 193 (2020) 112178. https://doi.org/10.1016/j.ejmech.2020.112178.

[46] K. Flentie, G.A. Harrison, H. Tükenmez, J. Livny, J.A.D. Good, S. Sarkar, D.X. Zhu, R.L.

Kinsella, L.A. Weiss, S.D. Solomon, M.E. Schene, M.R. Hansen, A.G. Cairns, M. Kulén, T. Wixe, A.E.G. Lindgren, E. Chorell, C. Bengtsson, K.S. Krishnan, S.J. Hultgren, C. Larsson, F. Almqvist, C.L. Stallings, Chemical disarming of isoniazid resistance in Mycobacterium tuberculosis, Proc. Natl. Acad. Sci. U. S. A. 116 (2019) 10510–10517. https://doi.org/10.1073/pnas.1818009116.

[47] J.C. Stockert, R.W. Horobin, L.L. Colombo, A. Blázquez-Castro, Tetrazolium salts and formazan products in Cell Biology: Viability assessment, fluorescence imaging, and labeling perspectives, Acta Histochem. 120 (2018) 159–167. https://doi.org/10.1016/j.acthis.2018.02.005.

[48] D.S. Agarwal, V. Siva Krishna, D. Sriram, P. Yogeeswari, R. Sakhuja, Clickable conjugates of bile acids and nucleosides: Synthesis, characterization, in vitro anticancer and antituberculosis studies, Steroids. 139 (2018) 35–44. https://doi.org/10.1016/j.steroids.2018.09.006.

[49] J.C. Shelley, A. Cholleti, L.L. Frye, J.R. Greenwood, M.R. Timlin, M. Uchimaya, Epik: A software program for pKa prediction and protonation state generation for drug-like molecules, J. Comput. Aided. Mol. Des. 21 (2007) 681–691. https://doi.org/10.1007/s10822-007-9133-z.

[50] J.L. Banks, H.S. Beard, Y. Cao, A.E. Cho, W. Damm, R. Farid, A.K. Felts, T.A. Halgren, D.T. Mainz, J.R. Maple, R. Murphy, D.M. Philipp, M.P. Repasky, L.Y. Zhang, B.J. Berne, R.A. Friesner, E. Gallicchio, R.M. Levy, Integrated Modeling Program, Applied Chemical Theory (IMPACT), J. Comput. Chem. 26 (2005) 1752–1780. https://doi.org/10.1002/jcc.20292.

[51] S.K. Tripathi, R. Muttineni, S.K. Singh, Extra precision docking, free energy calculation and molecular dynamics simulation studies of CDK2 inhibitors, J. Theor. Biol. 334 (2013) 87–100. https://doi.org/10.1016/j.jtbi.2013.05.014.

[52] (2011) Protein Preparation, version 2.5, Epik, Schrödinger, LLC, New York, (n.d.).

[53] W. Sherman, T. Day, M.P. Jacobson, R.A. Friesner, R. Farid, Novel procedure for modeling ligand/receptor induced fit effects, J. Med. Chem. 49 (2006) 534–553.

https://doi.org/10.1021/jm050540c.

[54] R.A. Friesner, J.L. Banks, R.B. Murphy, T.A. Halgren, J.J. Klicic, D.T. Mainz, M.P. Repasky, E.H. Knoll, M. Shelley, J.K. Perry, D.E. Shaw, P. Francis, P.S. Shenkin, Glide: A New Approach for Rapid, Accurate Docking and Scoring. 1. Method and Assessment of Docking Accuracy, J. Med. Chem. 47 (2004) 1739–1749. https://doi.org/10.1021/jm0306430.

[55] (2011) Desmond, version 4.9, D. E. Shaw Research, New York., (n.d.).

[56] H.J.C. Berendsen, J.P.M. Postma, W.F. van Gunsteren, J. Hermans, Interaction Models for Water in Relation to Protein Hydration, in: Springer, Dordrecht, 1981: pp. 331–342. https://doi.org/10.1007/978-94-015-7658-1_21.

[57] W.G. Hoover, Canonical dynamics: Equilibrium phase-space distributions, Phys. Rev. A. 31 (1985) 1695–1697. https://doi.org/10.1103/PhysRevA.31.1695.

[58] Z. Ma, M. Tuckerman, Constant pressure ab initio molecular dynamics with discrete variable representation basis sets, J. Chem. Phys. 133 (2010) 44506. https://doi.org/10.1063/1.3499812.

[59] D.L. Beveridge, F.M. DiCapua, Free energy via molecular simulation: applications to chemical and biomolecular systems., Annu. Rev. Biophys. Biophys. Chem. 18 (1989) 431–492. https://doi.org/10.1146/annurev.bb.18.060189.002243.

[60] C. Jarzynski, Nonequilibrium equality for free energy differences, Phys. Rev. Lett. 78 (1997) 2690–2693. https://doi.org/10.1103/PhysRevLett.78.2690.

[61] X. Zhang, S.E. Wong, F.C. Lightstone, Toward fully automated high performance computing drug discovery: A massively parallel virtual screening pipeline for docking and molecular mechanics/generalized born surface area rescoring to improve enrichment, J. Chem. Inf. Model. 54 (2014) 324–337. https://doi.org/10.1021/ci4005145.

[62] J. Li, R. Abel, K. Zhu, Y. Cao, S. Zhao, R.A. Friesner, The VSGB 2.0 model: A next generation energy model for high resolution protein structure modeling, Proteins Struct. Funct. Bioinforma. 79 (2011) 2794–2812. https://doi.org/10.1002/prot.23106.